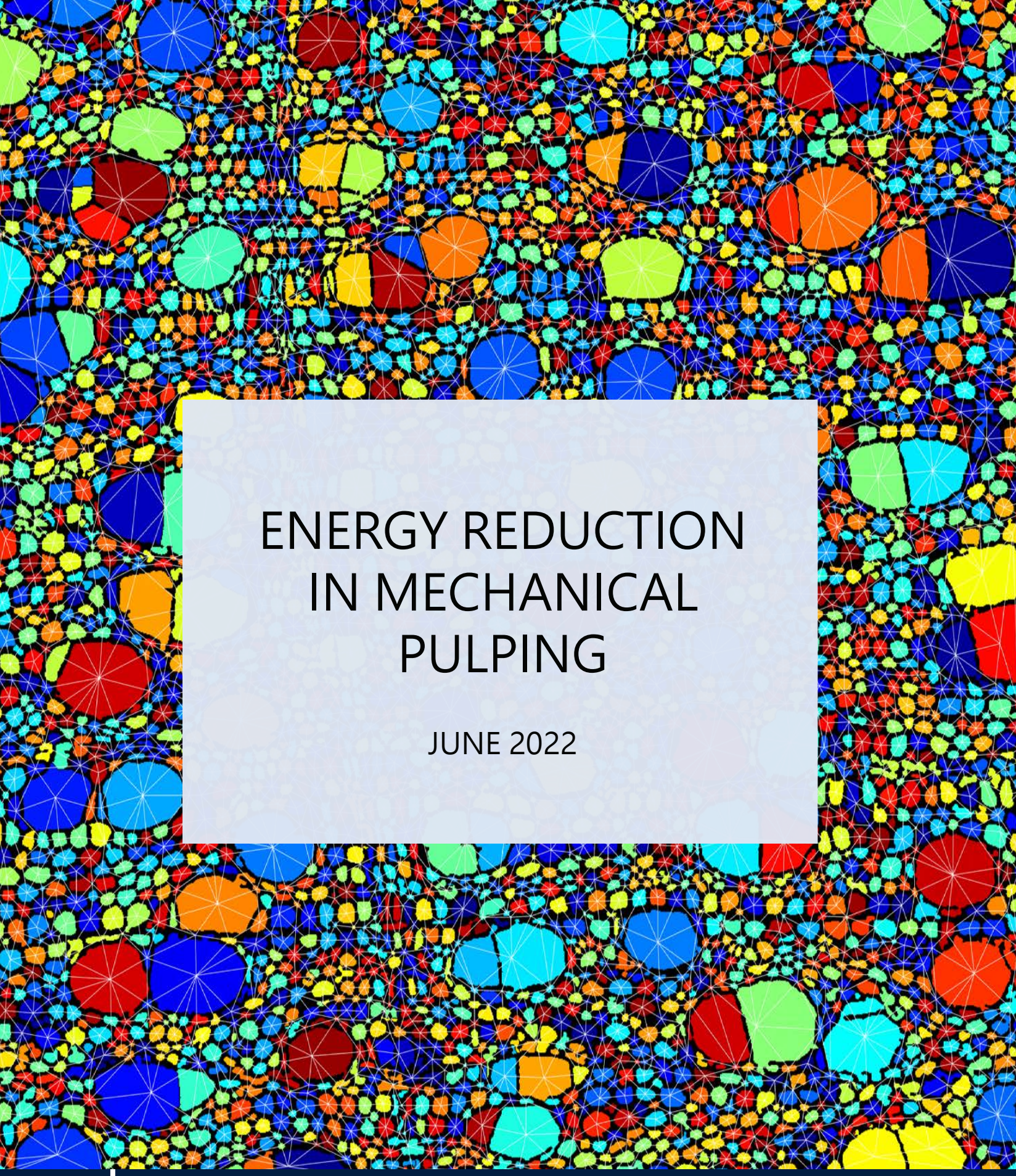

ENERGY REDUCTION IN MECHANICAL PULPING

JUNE 2022

THE UNIVERSITY OF BRITISH COLUMBIA

WELCOME MESSAGE

Dear partners in the Energy Reduction in Mechanical Pulping research program,

It is a great privilege for us to be part of a partnership that sees industry coming together around grand challenges such as energy conservation and improved technologies for the pulp and paper industry. Our research program continues to be in a unique position that brings together members from industry and academia to work together towards making lasting beneficial changes. One of the ongoing challenges continues to be the renewal of the workforce with those who will bring a strong understanding of technical fundamentals, and I believe this program allows us to build the next generation of industry leaders.

With the ease of travelling, I am pleased that for this opportunity, we can get together during the June 2022 Steering Committee Meeting happening in Vancouver. Thanks to all of you for actively participating during the past online meetings and providing valuable feedback to our students and researchers. I invite you to read the following pages with the progress for each project, and we look forward to providing you with a detailed update on each project's milestones on June 2nd.

As the year progresses we have had several personnel updates with new students joining the consortium and some farewells. Postdoctoral fellows, Mengqi Fang and Pierre Betu Kasangana, have left the program and continued with other career opportunities. We thank both for their contributions to the ERMP team and wish them great success in their future careers. Matthias Aigner has successfully defended his doctorate degree early this year and continues to participate in the program as a postdoctoral fellow. Additionally, we have also welcomed Co-op students at the PPC and BCIT: Ryan Hlina, Thomas Clarito, Stephen Lee, Renz Po, Priyanshi Shrivastava and returning student Samuel Brown. I invite you to review pages 36 to 38 for brief introductions to our new team members and their backgrounds, and other updates on the program.

I hope to see many of you at the June 2nd Steering Committee meeting and the International Mechanical Pulping Conference (IMPC) from June 5th to the 8th, both happening in Vancouver, British Columbia.

Sincerely yours,

Mark Martinez, Ph.D., P. Eng.,
Professor of Chemical and Biological Engineering, UBC
Principal Investigator, ERMP Research Program

CONTRIBUTORS

Matthias Aigner
Rodger Beatson
Samuel Brown
Yankai Cao
Siwei Chen
Thomas Clarito
James Drummond
Mengqi Fang
Elisa Ferreira
Mariana Frias de Albuquerque
Samira Gharehkhani
Bhushan Gopaluni
Pierre Betu Kasangana
Sudipta Kumar Mitra
Stephen Lee
Liyang Liu
Mark Martinez
Claire Maulit
James Olson
André Phillion
Renz Po
Scott Renneckar
Norman Roberts
Laurel Schafer
Priyanshi Shrivastava
Aurélien Sibellas
Boris Stoeber
Heather Trajano
Daniela Vargas Figueroa
Peter Wild
Cameron Zheng

MAILING ADDRESS
UBC Pulp and Paper Centre
2385 East Mall
Vancouver, BC V6T 1Z4

DESIGNER CONTACT
Program Manager
Daniela Vargas Figueroa
daniela.figueroa@ubc.ca
604-827-2390

CONTENTS

RESEARCH UPDATES

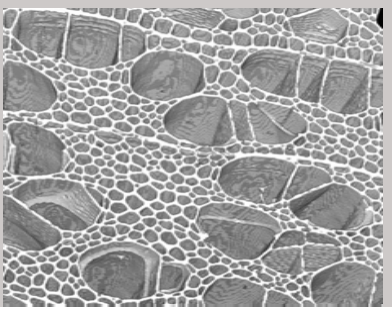

ON THE COVER

On the cover, is an image of a wood chip (original shown on the left) in which every lumen is labeled with a separate colour and its nearest neighbor by the white lines. This is a critical image processing step to characterize the size of the features in a wood chip. ***Authors:*** *Aurélien Sibellas, postdoctoral fellow and Samuel Brown, undergraduate COOP student.*

PROJECT 1.1

LC REFINING OF MECHANICAL PULP

Authors: Samira Gharehkhani, Matthias Aigner, James Olson, Peter Wild

Background

In previous work by researchers at the University of Victoria, a custom piezo-ceramic force sensor was developed to measure local shear and normal forces applied to the refiner bars. Sensors based on this design have been used in trials in a variety of high consistency (HC) [Olender et al. 2008] and low consistency (LC) [Harirforoush et al. 2018] refiners. Most recently, two different sets of trials were conducted at the Pulp and Paper Centre at UBC and the Catalyst, Paper Excellence mill in Crofton, BC [Aigner et al. 2020, Aigner et al. 2022]. The goal of these studies was to investigate the effect of operating conditions on radial distributions of force as characterized by the force profile during bar-passing events.

The trials conducted in the test refiner at UBC, show a transition from a single force peak to two peaks as refining energy increases [Aigner et al. 2020]. This transition has been shown, in previous work, to correspond to the onset of fiber cutting [Harirforoush et al. 2017]. This behaviour was also found in power curve trials at the Crofton refiner [Aigner et al. 2022]. Based on these results, the term *dual peak ratio* was introduced to describe the proportion of dual peak events out of all recorded bar passing events at a given refining condition. The authors assume that single peak events represent events where only friction force occurs while in dual peak events both corner force and friction force are present. Therefore, the dual peak ratio is thought to describe the prevalence of corner forces. Furthermore, it is shown that this dual peak ratio is affected by the radial position. Specifically, it was found that, at positions close to the axis and close to the periphery of the refiner, fewer dual peak events occur, while, between these regions, dual peak events are more prevalent [Aigner et al. 2022].

Trials set up

To expand on these previous findings, a comprehensive set of experiments is conducted to investigate the effect of refiner plate geometry, such as bar width and bar edge length (BEL), and refining parameters, such as specific edge load (SEL) and rotational speed, on bar force profiles and fibre and paper properties. An additional objective of these trials is to confirm and refine the bar force estimation model proposed by Kerekes and Meltzer [Kerekes et al. 2018]. The complete set of trials has the potential to extend the knowledge on LC refining of mechanical pulps and in doing that aid in the development of new refining plate design.

Table 1. Summary of the operating conditions for the pilot-scale LC refining trials

Table 1: Summary of the operating conditions for the pilot-scale LC refining trials

	Plate 002 BEL: 5.4 km/rev Bar width: 1.35 mm	Plate 003 BEL: 2.1 km/rev Bar width: 2.5 mm	New plate BEL: 2.1 km/rev Bar width: 1.35 mm
			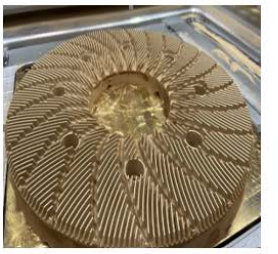
Rotational speed (rpm)	1200, 1600	1200, 1600	1200, 1600
SEL (J/m)	0.1, 0.2, 0.3	0.2, 0.4, 0.8	0.2, 0.4, 0.8
Consistency (%)	3.5	3.5	3.5
Flow rate (L/m)	250	250	250
Pulp type	Mechanical softwood pulp, Initial freeness 510 CSF		

PROJECT 1.1

The study comprises 18 trials in which three different refining plates are each run at two rotational speeds and three specific edge loads (SEL). Table 1 presents a summary of the trials. To investigate the impact of refiner plate design on fibre properties and force profiles, the third plate is designed so that it has the same BEL as one plate and the same bar width as the other plate.

As in our previous work, a sensor and an encoder were installed on the refiner machine to record the bar forces and reference these to the position of the rotor with respect to the bar force sensor.

Results

Refining operating conditions

Figures. 1 (a and b) present the effect of rotational speed and the SEL on the net power and gap for plates No. 002 and No. 003, respectively. The net power and gap data are presented as the average net power and average gap data of all sample points during each refining trial. SEL is a common measure of the refining intensity and represents energy expended per bar crossing per unit bar length [Kerekes et al. 2006]. SEL is defined as net power divided by the product of BEL and rotational speed. As can be seen in Fig. 1a and 1b, the power-gap curves are shifted to the right with an increase in rotational speed. This is in accordance with prior studies (Berna et al. 2019, Elahimehr et al. 2013, Luukkonen et al. 2010) For instance, Elahimehr et al. (2013) showed that the power-gap relationship is strongly affected by angular velocity and that at a high angular velocity significantly higher powers can be reached at the same gap. Recently, Berna et al. (2019) presented a dimensionless power number that can be used to describe refining power, as well as to predict refining gap. We aim to provide such dimensionless numbers by conducting pulp refining under various conditions. Further information will be provided upon analyzing the fibre and paper properties.

Force Sensor

Based on previous work, the dual peak ratio was evaluated for each trial at each sample point and plotted against SEL in Figure 2, for plate 003, and Figure 3, for plate 002. For plate 003 the dual peak ratio for trials run at 1600 rpm trends downwards with increasing SEL in both the normal (Figure 2 (a)) and shear force (Figure 2 (b)) plots. For the 1200 rpm trials the dual peak ratio increases with increasing SEL in both plots (Figure 2 (a) and (b)). The crossover point of these two trend lines appears for the normal force plot at SEL 0.2 and in the shear force plot at SEL 0.4.

For plate 002 the dual peak ratio increases for both 1200 and 1600 rpm trials with increasing SEL (Figure 3). In the normal force plot (Figure 3 (a)) the dual peak ratio is higher for the 1200 rpm trial except at SEL 0.3 while for the shear force plot (Figure 3 (b)) the dual peak ratio is the highest for all 1200 rpm trials.

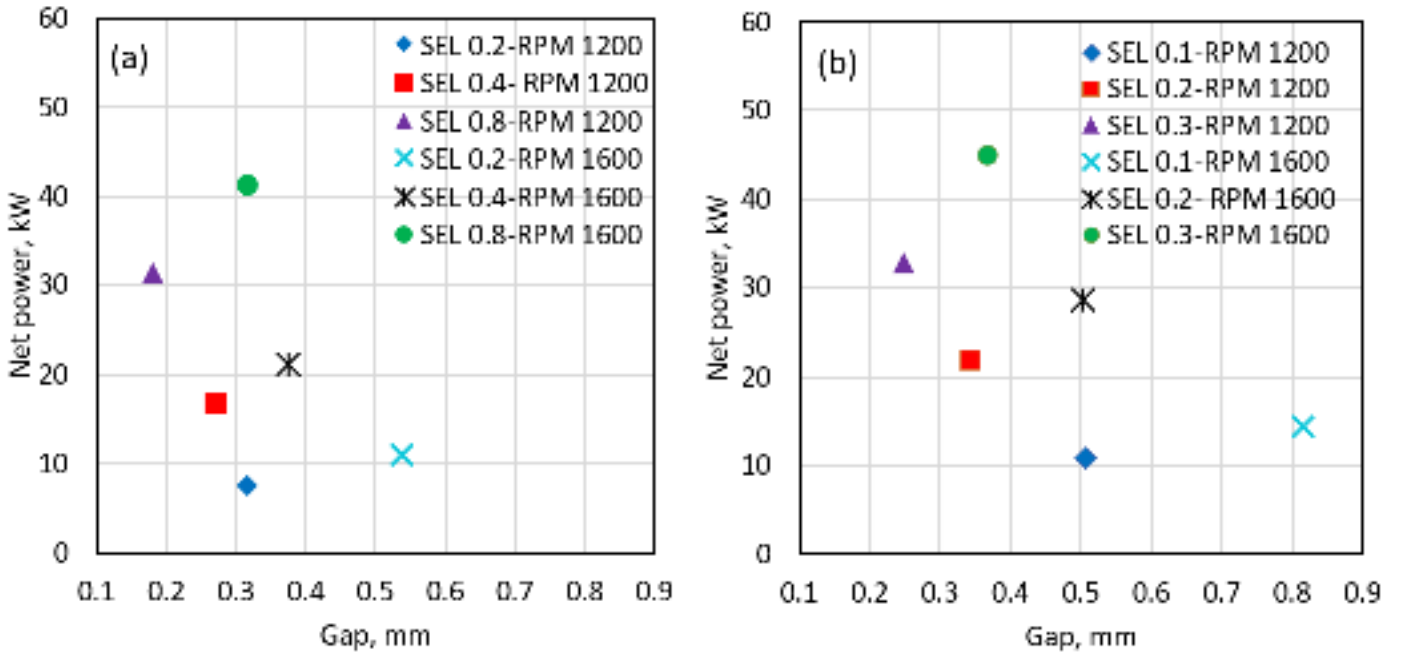

Figure 1. Experimental data of net power versus gap for different rotational speed and SEL values a) plate 002, and b) plate 003

PROJECT 1.1

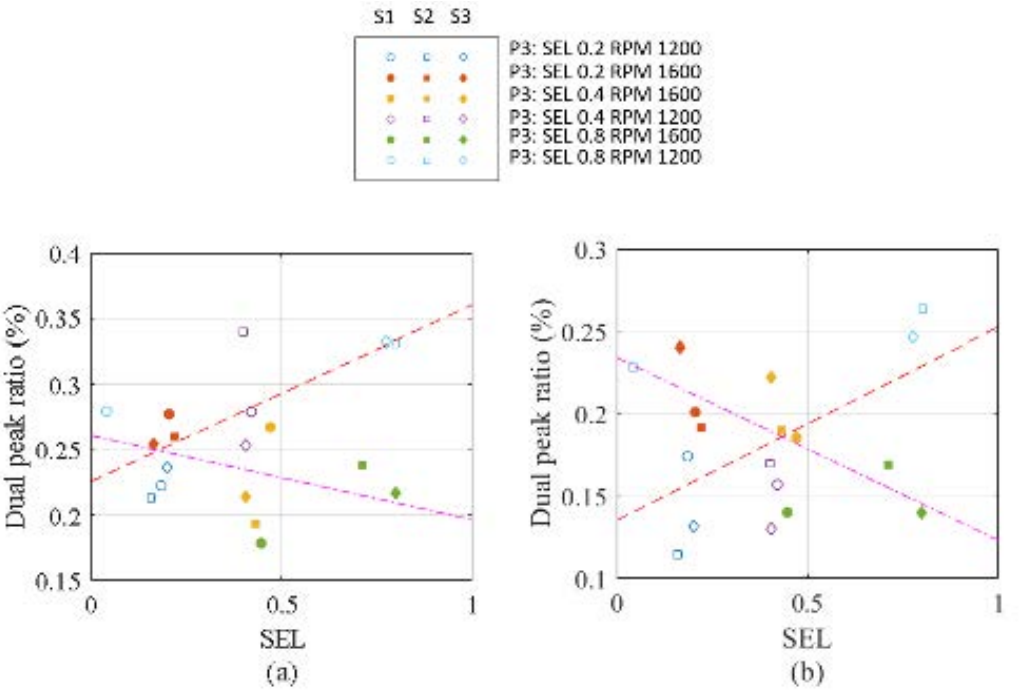

Figure 2. Dual peak ratio plotted over SEL for trials on plate 003 for normal (a) and shear force (b). Each trial is represented by a separate colour, and sample points 1-3 in each trial are represented by circle, square and diamond shapes respectively. Trials at 1200 rpm are not filled in whereas trials at 1600 rpm have filled in data points. The trend lines for the 1200 rpm data points are included in red and a dashed line; the ones for the 1600 rpm data point in a pink dash-dotted line.

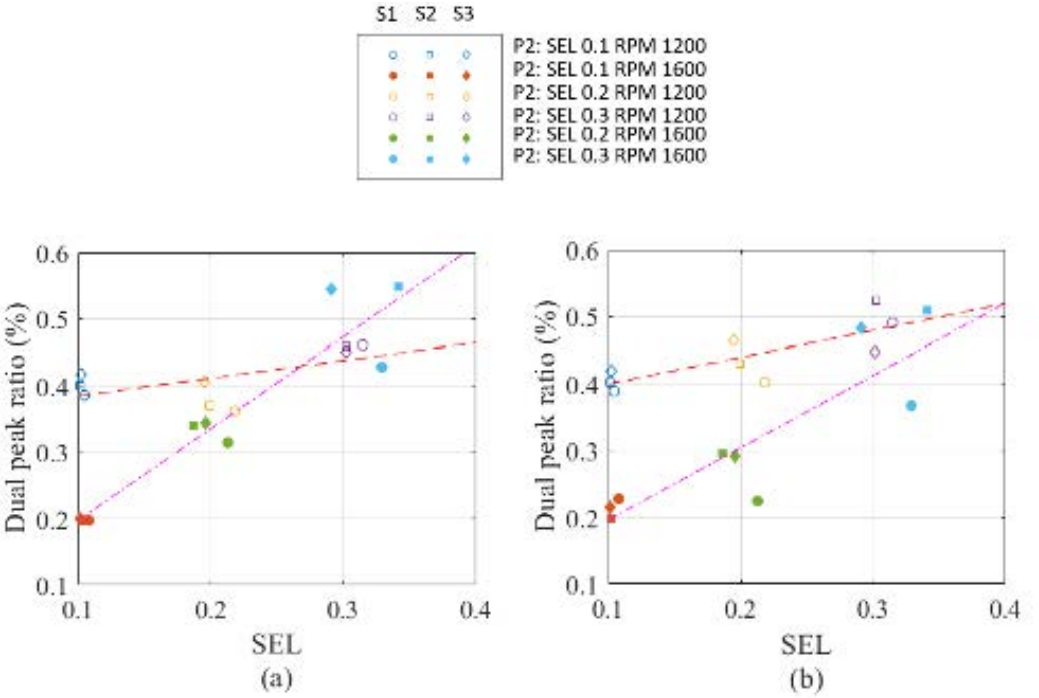

Figure 3. Dual peak ratio plotted over SEL for trials on plate 002 for normal (a) and shear force (b). Each trial is represented by a separate colour, sample points 1-3 in each trial are represented by circle, square and diamond shapes respectively, trials at 1200 rpm are not filled in whereas trials at 1600 rpm have filled in data points. The trend lines for the 1200 rpm data points are included in red ad a dashed line and the ones for the 1600 rpm data point in a pink dash-dotted line.

PROJECT 1.1

The dual peak analysis shows that there are trends in the dual peak ratio. Except for the trials at 1600 rpm at plate number 003 the dual peak ratio increases with increasing SEL. These trends can be interpreted as being consistent with the Crofton results. While the authors theorize that the difference in trends is due to a change in bar passing mechanism because of different tangential speeds and geometry, the exact mechanism for this trend is not understood at this time.

Future Research

Two of the three planned trial sets have been completed so far. The third trial set will be continued using the new plate design that shares the same BEL with plate No. 003 and the same bar width as plate No. 002. This will allow the investigation of the effect of bar design on the fiber and paper properties in detail. Moreover, the recorded forces will be compared with the model proposed by Kerekes and Meltzer. Furthermore, the fibre property data will be included in the analysis.

Acknowledgments

The authors thank Mr. Roberts Norman for conducting the refining trials.

References

1. Aigner, M., Olson, J., and Wild, P. (2020). Measurement and interpretation of spatially registered bar-forces in LC refining. Nordic Pulp & Paper Research Journal, 35(4), 600-610.
2. Aigner, M., Olson, J., Sun, Y., and Wild, P. (2022). Interpretation of force profiles in mill-scale LC refining. Nordic Pulp & Paper Research Journal, 37(1), 42-53.
3. Berna, J. E. R., Martinez, M., & Olson, J. (2019). Power–gap relationships in low consistency refining. Nordic Pulp & Paper Research Journal, 34(1), 36-45.
4. Elahimehr, A., Olson, J. A., & Martinez, D. M. (2013). Understanding LC refining: The effect of plate pattern and refiner operation. Nordic Pulp & Paper Research Journal, 28(3), 386-391.
5. Harirforoush, R, Olson, J., and Wild, P. (2017). In-Process Detection of Fiber Cutting in Low Consistency Refining Based on Measurement of Forces on Refiner Bars. Tappi Journal 16 (4): 460–69.
6. Kerekes, R. J., & Senger, J. J. (2006). Characterizing Refining Action in Low- Consistency refining. Journal of pulp and paper science, 32(1).
7. Kerekes, R., and Meltzer, F. (2018). The influence of bar width on bar forces and fibre shortening in low consistency pulp refining. Nordic Pulp & Paper Research Journal, 33(2), 220-225.
8. Luukkonen, A., J. A. Olson, and D. M. Martinez. Low consistency refining of mechanical pulp, effect of gap, speed and power. Journal of Pulp and Paper Science 36.1-2 (2010): 28-34.
9. Olender, D., Wild, P., & Byrnes, P. (2008). A piezoelectric force sensor for mill-scale chip refiners. Proceedings of the Institution of Mechanical Engineers, Part E: Journal of Process Mechanical Engineering, 222(2), 115-122.

PROJECT 1.2

PULP QUALITY AND MODELING AND PROCESS OPERATING REGION EVALUATION IN THE THERMOMECHANICAL PULPING PROCESS

Authors: Mengqi Fang, Bhushan Gopaluni, Yankai Cao.

Background

In the Chemi-Thermomechanical Pulping (CTMP) process, the pulp refining processes, including the high consistency and reject refining, are considered the core operating units due to their direct effect on the pulp properties. Significant research has been done to identify the correlations between the refiner operating conditions and product properties with the hope of improving the operational efficiency. We are interested in optimizing the total specific energy (TSE) consumption while maintaining the pulp properties (Harinath, Biegler and Dumont 2011). This optimization requires a high-fidelity model that relates various process variables with TSE. However, due to the complicated, dynamic and time-varying characteristics of refining processes, building such a model is not an easy task. Therefore, as a first step, we developed different types of models and compared them to identify the best among them. Using these models, an ideal set of operating conditions were identified for the manipulated variables. Finally, the real-time operating performance of the entire refining process is summarized according to the estimated pulp quality and the potential TSE reduction.

Figure 1 below summarizes our approach which includes four stages. The process operating variables, frequently sampled pulp properties, such as freeness, and infrequently sampled handsheet properties, such as tensile, are modeled separately. The modeling procedures and the related performance measures are presented below in Parts 1 & 3. Using these models, we developed an approach for evaluating various operating regions and it is explained in Part 2. A reliability analysis of the models is also developed and presented in Part 4.

Results

Part 1: Modeling of frequently sampled pulp properties

In order to model the correlation between the process operating variables and the pulp properties, a simple but effective model structure has been employed and updated every sampling instant by using historical data in a fixed moving window. Two frequently sampled pulp properties are selected as the model outputs and the following ARX models are employed, where q_1 and q_2 represent the two pulp properties and X indicates all the selected process operating variables with time delay d. β_1 and β_2 are two model parameter vectors which are estimated and updated at every sampling instant.

$$q_1(t) = [q_1(t-1), q_2(t-1), X(t-1:t-d), 1] \cdot \beta_1(t-1)$$

$$q_2(t) = [q_1(t-1), q_2(t-1), X(t-1:t-d), 1] \cdot \beta_2(t-1)$$

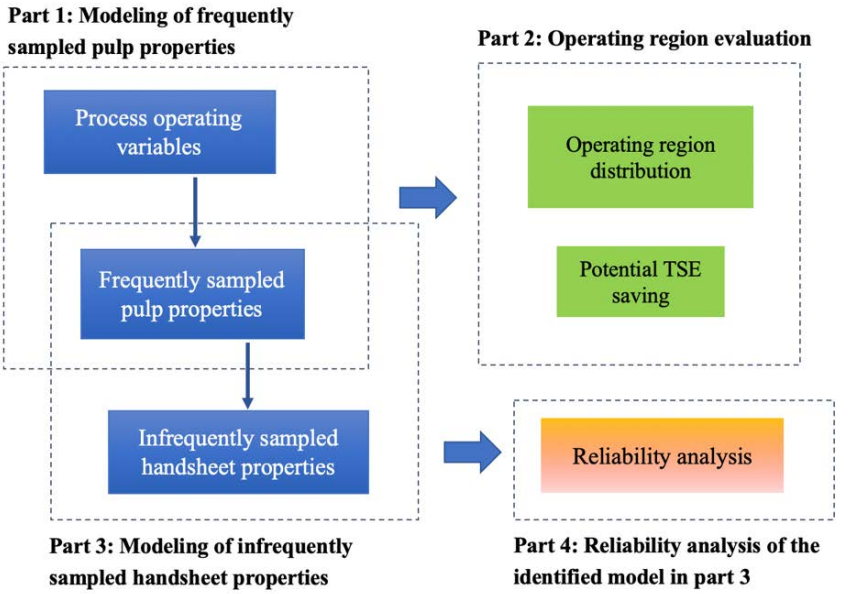

Figure 1. The workflow of this study.

PROJECT 1.2

The performance of the estimated models is validated on the real mill operating data set. As shown in Figure 2, the model output and the actual measurements are highly correlated and the normalized RMSE of q_1 and q_2 are computed as 0.0215 and 0.1582, respectively, which indicates a satisfactory modeling performance.

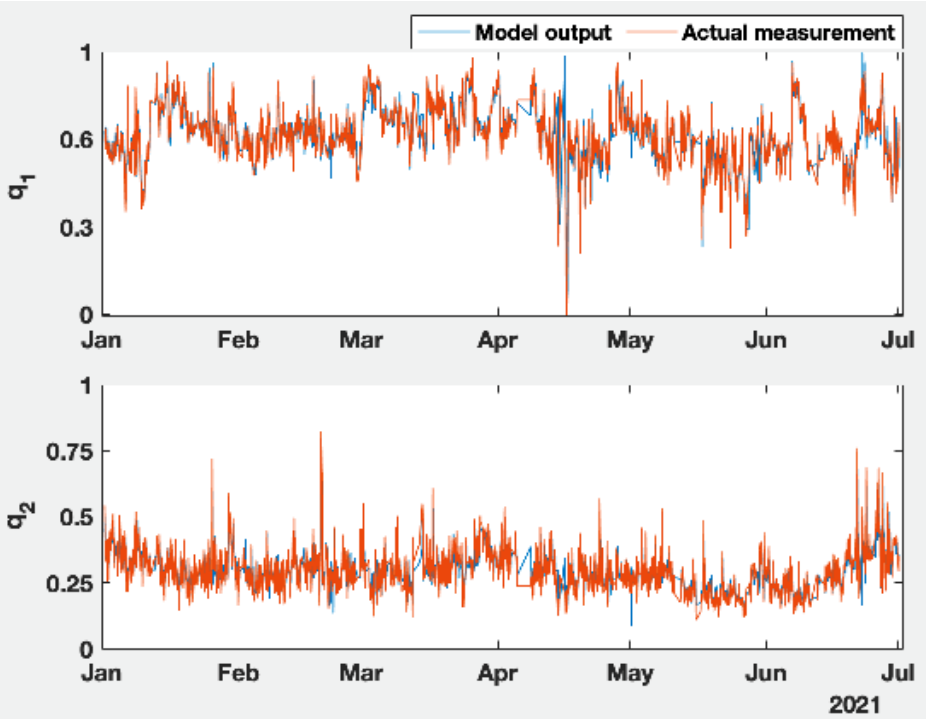

Figure 2. Model validation performance of the two selected pulp properties after normalization.

Part 2: Operating region evaluation

Based on the above ARX models, one can explore the measurement space of selected process operating variables by generating uniformly distributed random samples as model inputs. Then the model outputs q_1 and q_2 are evaluated based on the product property constraints.

Figure 3 illustrates one way to segment possible pulp quality regions, where q_1 is expected to lie between the q_1 upper and lower bounds, and q_2 is expected to be no larger than the designated q_2 upper bound. In this case, the labeled green region 1 is the desired pulp quality region, whereas the other pulp quality regions labeled by different colors are to be avoided. We are interested in finding the best way to distribute TSE between the primary and secondary refiners. Using α to denote the fraction of TSE applied to the primary refiner, we can write the following constraints:

$$SE_{p,lower} \leq TSE \cdot \alpha \leq SE_{p,upper}$$
$$SE_{s,lower} \leq TSE \cdot (1-\alpha) \leq SE_{s,upper}$$

where $SE_{p/s,upper}$ and $SE_{p/s,lower}$ indicate the upper and lower bound of primary and secondary refiner specific energies, respectively.

After comprehensively exploring the sample space of TSE and α, a 2D feasible map is created and illustrated in Figure 4. Here, corresponding to the TSE and α values, the model predicted $(\hat{q}_2, \hat{q}_1)$ pair is labeled by the region number and color according to Figure 3, and the black diamond shows actual process operating status and pulp quality. The distribution of multiple regions in Figure 4 is summarized in Table 1, which can also be interpreted as the probability of the process spending time in that region. In other words, the longer a process spends in region 1, the more likely that it produces desired pulp products. Additionally, the dark shaded green area in Figure 4 represents operating regions with lower TSE consumption.

PROJECT 1.2

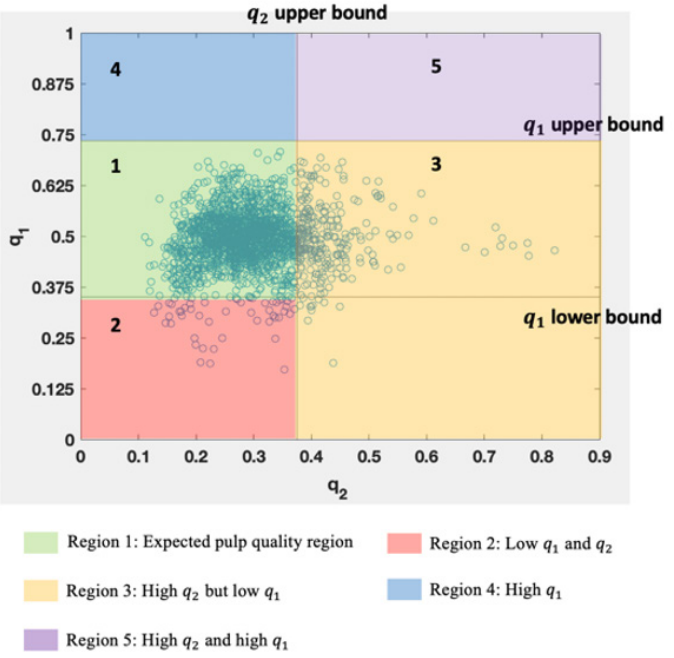

Figure 3. An illustration of pulp quality region segmentation

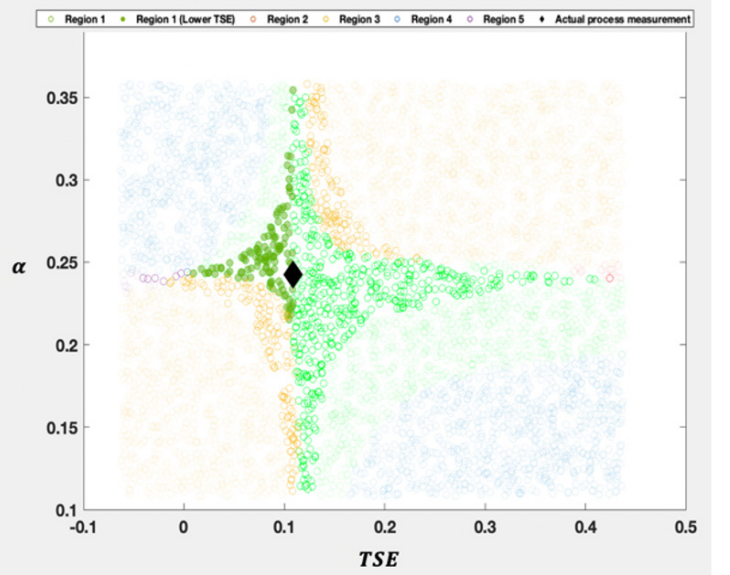

Figure 4. 2D feasible map

Table 1. The distribution of multiple pulp quality regions.

Quality region	Region 1	Region 2	Region 3	Region 4	Region 5
Percentage	68.32%	0.12%	30.75%	0.12%	0.69%

Part 3: Modeling of infrequently sampled handsheet properties

Similar to the modeling strategy explained in Part 1, linear model structure is employed when performing modeling of infrequently sampled handsheet properties. The model inputs and outputs are included in the following equations, where h₁ and h₂ represent the selected handsheet properties, Q indicates all the other infrequently sampled quality variables, and q₁ is the frequently sampled pulp property variable. The model input features are selected and computed following the PhD dissertation (Qian 1996). With this model structure, a PLS regression model (de Jong 1993) is employed and model parameters are estimated. The statistics of model performance are summarized in Table 2.

$$z(t) = [h_1(t-1), h_2(t-1), Q(t-1), q_1(t)]^T$$

$$h(t) = [h_1(t), h_2(t)]^T$$

Table 2. The statistics of model prediction performance.

Statistics	R^2 value	Normalized RMSE	Correlation coefficient of the model output and actual measurement
Handsheet property h_1	0.5705	0.1334	0.7649
Handsheet property h_2	0.4930	0.0839	0.7069

PROJECT 1.2

Part 4: Reliability analysis of the model identified in Part 3

The identified model in Part 3 is used to generate real-time predictions of the infrequently sampled handsheet properties, which are normally sampled in days or even weeks. Therefore, it is important to quantify the reliability of this model. By using probabilistic models between the prediction error e and the frequently sampled model input q_1, a novel reliability measurement index is proposed in the following equation:

$$R_t(q_1) = P(|e| \le th|q_1, D) \cdot P(r = 0|q_1, D) - P(|e| > th|q_1, D) \cdot P(r = 1|q_1, D)$$

where th is the manually set threshold to classify the model reliability based on the absolute error value, and r denotes the reliability status of this model given q_1 and historical data D, where r=0 indicates the model falls into more reliable region and r=1 implies the model is less reliable.

When the reliability index R_t is less than or equal to zero, it indicates that the model is less reliable than for a positive R_t. As a validation, Table 3 summarizes the actual prediction error distribution with different R_t values. From this result, we can clearly observe that when $R_t \le 0$, there are more than 35% of samples resulting in larger absolute errors, which is much higher than the errors when $R_t > 0$ case.

Table 3. The reliability analysis validation.

Prediction error	$R_t > 0$	$R_t \le 0$
$\|e\| \le th$	72.26%	51.61%
$th < \|e\| < 1.5th$	16.99%	12.90%
$\|e\| \ge 1.5th$	10.75%	35.48%

Conclusions and Future work

Focusing on the core high consistency refining units in CTMP process, we modelled frequently sampled pulp properties and infrequently sampled handsheet properties. Using a model, the sample space of selected process operating variables is explored and evaluated by inspecting the predicted pulp qualities, and a reliability index is developed to monitor the model prediction accuracy in real time. This work has been validated using the most recent mill data. Our eventual goal is to use these tools to provide helpful guidelines on how to operate the mill so as to optimize energy consumption without compromising on the quality of the products.

With Mengqi's departure in late 2021, we have made an offer to a new postdoctoral fellow, Vijay Kumar Pediradla, who will be joining us middle of summer this year.

References

1. de Jong, Sijmen. 1993. "SIMPLS: An Alternative Approach to Partial Least Squares Regression." Chemometrics and Intelligent Laboratory Systems 251–63.
2. Harinath, Eranda, L. T. Biegler, and Guy A. Dumont. 2011. "Control and optimization strategies for thermo-mechanical pulping processes: Nonlinear model predictive control." Journal of Process Control 21 (4): 519-528.
3. Qian, Xingsheng. 1996. "Modelling and dynamic simulation of CTMP plant." Dissertation University of British Columbia.

PROJECT 1.3

CREATING LOW ENERGY SHIVE-FREE PULPS

Authors: Sudipta Kumar Mitra, Claire Maulit, Rodger Beatson, Heather Trajano

Background

Research performed by Chang et al. has shown that oxidative chemical pretreatment followed by low consistency refining can increase strength gains while alleviating energy consumption. For example, a fully HC-refined hemlock TMP requires about 2,000 kWh/t to reach a tensile index of 38 Nm/g. But a primary HC-refined softwood pulp treated with alkaline peroxide at charges of 4% H_2O_2 and 6% NaOH, then low-consistency refined, needs only 1000 kWh/t. Similar findings exist for chlorine dioxide and ozone.

The mechanisms of paper strength gains and development of other properties due to oxidative agents have been proposed in literature and previous experimental works:

- In **highly alkaline peroxide treatment (HAPT)**, the strength gain is hypothesized to be mainly due to the generation of acid groups on the surface of fibres and fines which increases surface charge and causes surface fibre swelling. The swelling increases the bonded surface area and causes sheet densification.
- **Chlorine dioxide** oxidizes lignin to produce carboxylic acids. When combined with an alkali soak, the sodium salt formation can lead to softening and swelling of the fibres and fines and thus increases tensile strength.
- **Ozone treatment** acts in a similar manner to chlorine dioxide by forming carboxylic acids which, after an alkali soak, cause softening of the fibres and fines leading to increased tensile strength.

Previous Work

In November 2021, we reported on HAPT handsheet properties and pulp settling behaviour. HAPT treatment increased tensile strength of second stage TMP from 26 Nm/g to 47 Nm/g. Reduction in bulk and increase in tensile strength were observed during the forming and early pressing stages of handsheet making. Higher alkali charge was correlated with greater pulp consolidation as determined by settling tests. These consolidations suggested that HAPT fines contribute to paper strength development.

Objectives

The broader objectives of this project are to: (1) generate a better understanding of the impact of chemical/biological treatments on development of fibre and fines properties during LC refining, and (2) develop economically viable low-energy processes that combine the use of such treatments with LC refining to produce printing/writing and board grades. Since November 2021, we have investigated the strength development mechanisms by HAPT.

Experimental

A secondary refiner TMP (60% Spruce/40% Pine) of CSF 390 mL was treated with 4% hydrogen peroxide, 6% NaOH, and 3% Na_2SiO_3 for 2 hours at 75 ˚C and 20% consistency. The acid group and surface charge of the pulp was determined after it was washed with deionized water. Fines were recovered by washing the pulp with 16 L of deionized water over a 200-mesh screen affixed to a shive analyzer.

Acid Group Analysis

For sample preparation, 3 g OD of pulp was soaked in 0.1 M hydrochloric acid to convert the acid groups into their protonated form. The pulp was then washed to constant conductance and dispersed in 0.001 M NaCl solution. 5 mL of 0.1 M HCl is added to account for the lack of strong acid groups on the Secondary refined pulp. Conductometric titration with alkali titrant (0.1 M NaOH) was performed to generate a titration curve and determine two equivalence points representing the strong acid groups and the total acid content. A nitrogen gas atmosphere was maintained to prevent interference from carbon dioxide in the air.

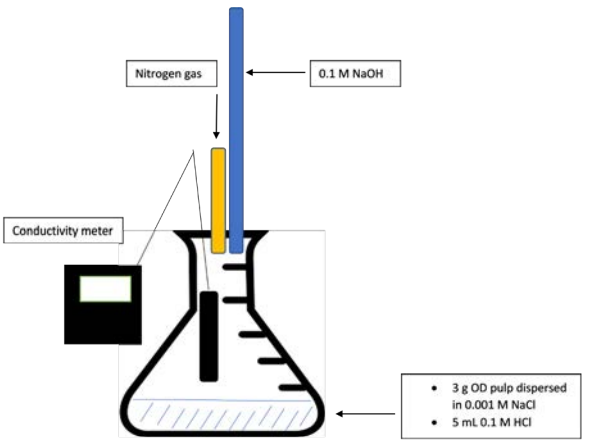

Figure 1. Acid group analysis apparatus

PROJECT 1.3

Surface Charge Measurement

Direct titration was performed using the Mutek PCD 03 titrator with cationic titrant Poly-DADMAC (0.001 mol/L). 10 mL of 0.3% consistency pulp was deposited into the vessel and a 30-minute run time was allowed to reach a steady reading. Afterwards, the specific charge, q, was calculated by using the titrant volume, concentration, and sample mass.

$$q\left[\frac{eq}{g}\right] = \frac{titrant\ volume\ x\ concentration}{mass\ of\ sample}$$

Kinetics study of strength development by HAPT

To determine the strength development kinetics of mechanical pulp by HAPT we used Holmens Braviken pulp (195 CSF). The chelated pulp samples were treated at 20% consistency with chemical charging: 2% H_2O_2, 6% NaOH, 3% Na_2SiO_3 at three temperatures: 65˚C, 75˚C, 85˚C (not completed). Treatment time was varied from 0 to 120 mins, handsheets were prepared and physical properties were measured. The sampling point for 0 min was heating the pulp sample in the water bath to 65˚C and 75˚C respectively, then adding chemicals, mixed and washed right after mixing chemicals.

Results

Acid Group Analysis

The figures below are examples of the titration curves of the untreated second-stage TMP (control) and HAPT treated fibres. The graphs plot conductance versus cumulative volume of added titrant.

The first linear portion of the curve shows a decrease in conductivity due to the titration of the added 5 mL HCl. The horizontal portion of the curve represents the titration of the weak carboxylic acid groups attached to the fibres and fines. The final segment reflects addition of excess sodium hydroxide.

Two equivalence points are found at the intersections of the extrapolated lines. The carboxylic acid concentration is determined from the difference between the strong acid content, A, and the total acid content, B, and is reported per unit weight of pulp.

The carboxylic acid group content was measured for the control pulp, the HAPT pulp, and the respective long fibre fractions. The HAPT approximately doubled the acid group content in the whole pulp and the long fibres. The difference between the whole pulp and the long fibre acid content reflects the acid group content of the fines.

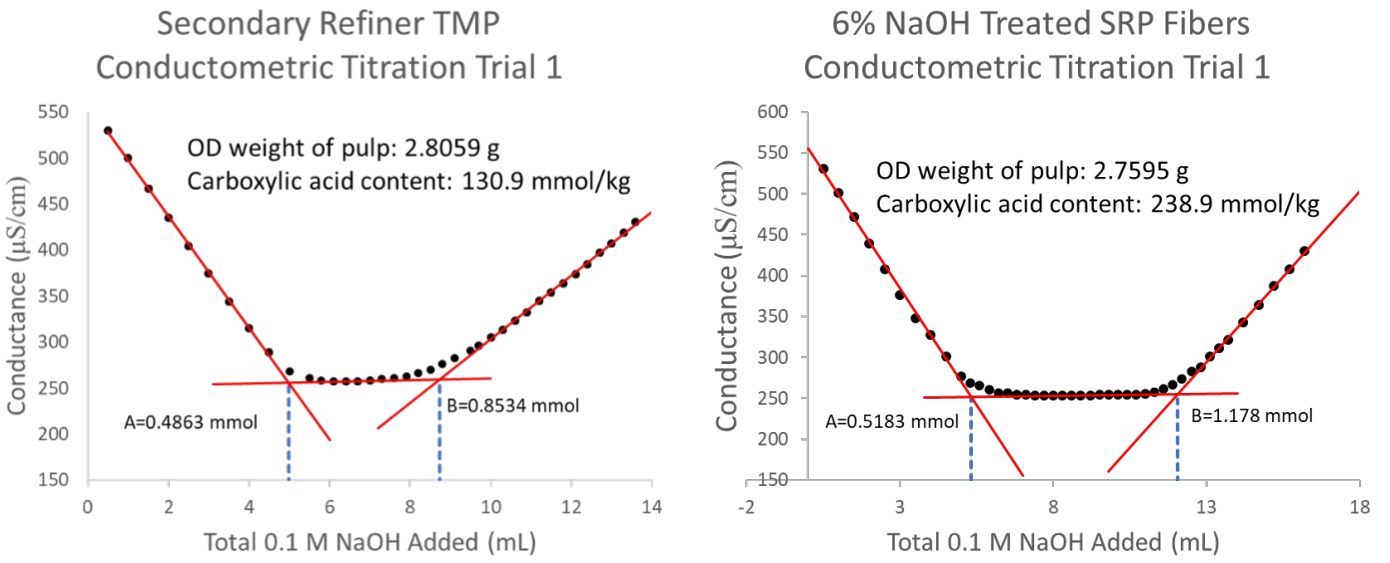

Figure 2. Titration curve for control SRP (left) and HAPT SRP fibres (right).

PROJECT 1.3

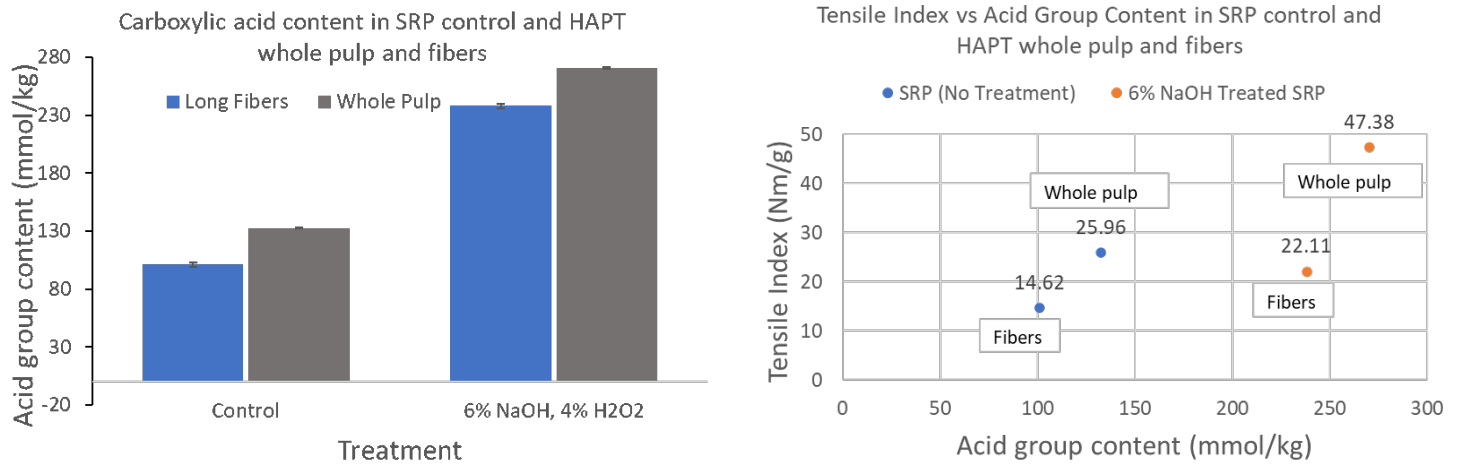

Figure 3. Carboxylic acid content of control and HAPT SRP for both the whole pulp and long fibres (left) and tensile index vs. acid group content (right)

The handsheet tensile indices increase with increasing acid group content providing further support that strength gains from HAPT are in part explained by the acid groups.

Surface Charge Measurement

Comparing the surface charges in the control whole pulp, HAPT pulp, and corresponding long fibres, the specific charge or surface charge increases when HAPT was applied to the second-stage TMP. The majority of surface charge is associated with the long fibres for both the control and HAPT pulp.

The increase in surface charge follows the trend seen in the acid group generation in HAPT pulp and long fibres. Increased surface charge seems to contribute to the fibre-fibre interactions and thus the overall strength development in HAPT.

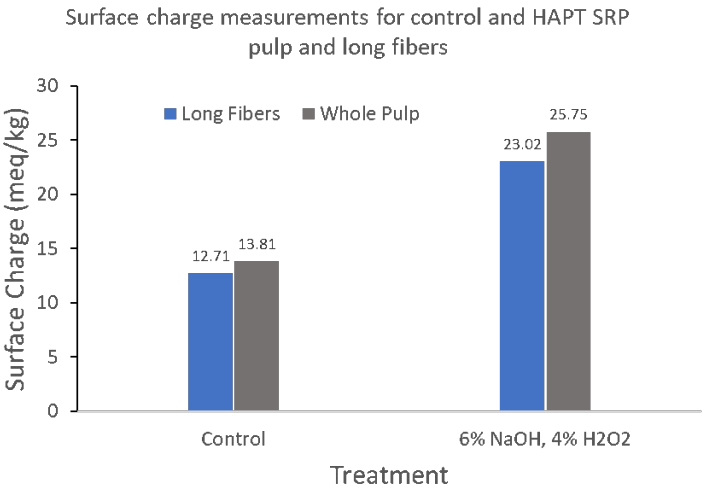

Figure 4. Surface charge of control for both pulp and long fibers and after HAPT.

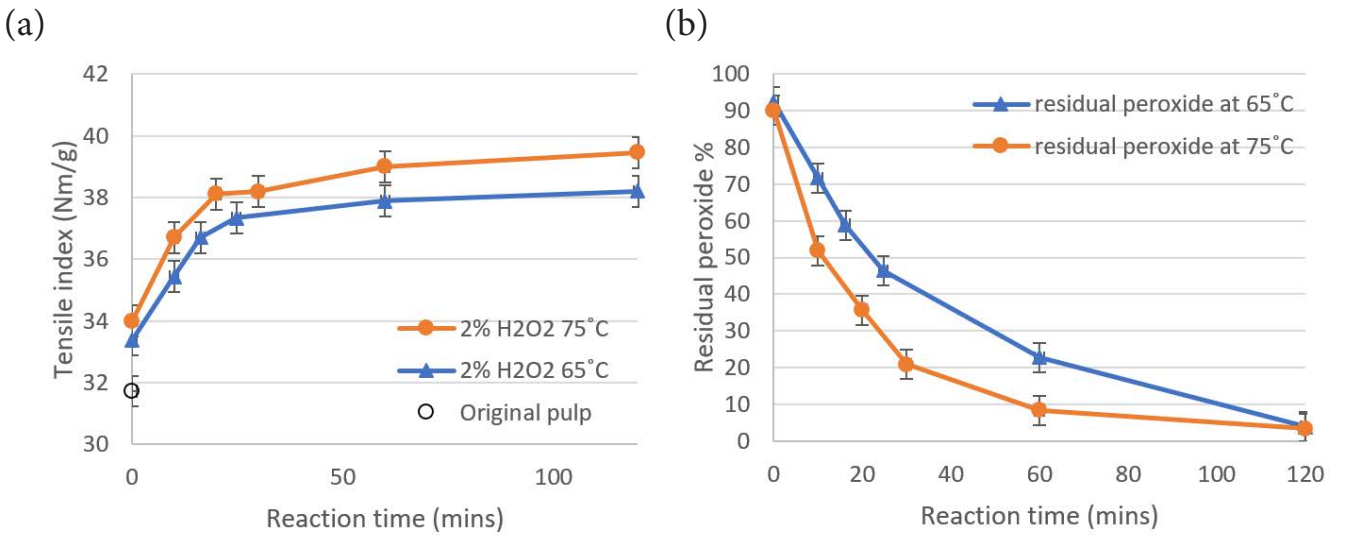

Figure 5. (a) Tensile strength as a function of HAPT time at 65°C (blue triangles) and 75°C (orange circles). (b) Residual peroxide (wt%) as a function of reaction time

PROJECT 1.3

Kinetics Study of strength development by HAPT

Figure 5a shows a rise in tensile strength with treatment time at both 65˚C and 75˚C. Initially there is a rapid increase in strength followed by a plateau. Greater tensile strength is achieved at 75˚C. Figure 5b shows that the residual peroxide content decreases more rapidly at 75˚C compared to 65˚C reflecting increasing reaction rate and/or peroxide decomposition with increasing temperature.

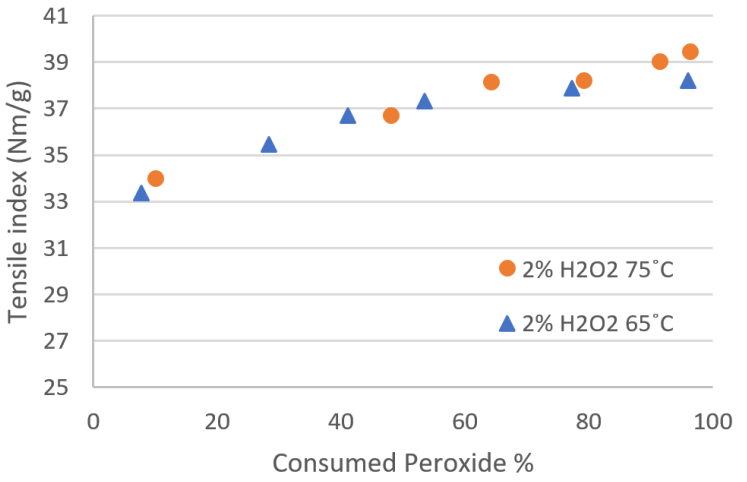

Figure 6. Tensile strength increases with peroxide % consumed during reaction

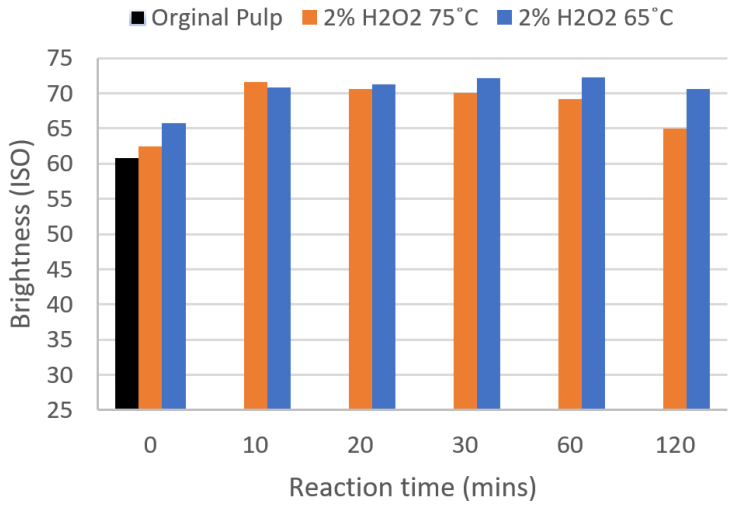

Figure 7. Change in brightness with reaction time

In figure 6, tensile strength increases with increasing hydrogen peroxide consumption implying that strength gains are dependent on the oxidation of the pulp with hydrogen peroxide.

Figure 7 presents brightness as a function of treatment time using 2% hydrogen peroxide. The brightness of the original pulp is represented by the black bar. Brightness increases after 10 min of treatment. At 65˚C, there is little change with time beyond 10 min. At 75˚C brightness decreases between 60 min and 120 min, possibly due to the negligible amount of peroxide remaining.

All these observations demonstrate the importance of temperature and time for strength development.

Future Research

In future work, the role of the HAPT fibres and fines in sheet consolidation and strength development will be further investigated by preparing handsheets in which the ratio of fines to fibres is varied over a wide range. The role of fines and fibres in strength development for chlorine dioxide and ozone treated mechanical pulps will be determined. The kinetics of strength development during HAPT treatment at 85˚C will be investigated.

The suitability of pulp subjected to oxidative chemistry (chlorine dioxide and ozone) for use in products such as paperboard, printing papers, and flexible packaging, will be further evaluated.

References

1. X. F. Chang, A. Luukkonen, J.A. Olson, R.P. Beatson, “Pilot-Scale investigation into the effects of alkaline peroxide pre-treatments on low-consistency refining of primary refined softwood TMP“, BioResources, 11(1), 2030-2042, 2016.
2. X. F. Chang, C. Bridges, D. Vu, D. Kuan, L. Kuang, J. A. Olson, A. Luukonen and R. P. Beatson, "Saving Electrical Energy by Alkaline Peroxide Treatment of TMP prior to Low Consistency Refining," Journal of Pulp and Paper Science, vol. 36, pp. 129-134, 2010.
3. S. Moldenius, "The Effects of Peroxide Bleaching on the Strength and Surface Properties of Mechanical Pulping,” Journal of Pulp and Paper Science., vol. 10, pp. 172-177, 1984.
4. J. R. Presley and R. T. Hill, "Peroxide bleaching of (chemi)mechanical pulps," in Pulp Bleaching: Principles and Practice, C. W. Dence and D. W. Reeve, Eds. Atlanta, Georgia: TAPPI, 1996, pp. 457-489.
5. A. Korpela, "Improving the Strength of PGW Pine Pulp by Alkaline Peroxide Treatment," Nordic Pulp and Paper Research Journal, vol. 17, pp. 183-186, 2002.
6. J. Been, "A Novel Approach to Kinetic Modeling of the Hydrogen Peroxide Brightening of Mechanical Pulp," Tappi Journal, pp. 144-152, 1995.
7. P. Engstrand, B. Sjogren, K. Olander and M. Htun, "The significance of carboxylic groups for the physical properties of mechanical pulp fibers," in 6th International Symposium Wood Pulping Chemistry, 1991, pp. 75-79.

PROJECT 2.1

LIGNIN RICH FINES: SIMPLE ROUTES TOWARDS CREATION OF HYDROPHOBIC AND HYDROPHILIC FILLER ADDITIVES

Authors: Liyang Liu, Siwei Chen, and Scott Renneckar

Background

An emerging bioeconomy is motivating the thermomechanical pulp industry to valorize their major side products, incldluing fines which can be up to 30 wt% of their pulping products. [1] Potentially, these small wood particles (<75 μm) can be valorized by producing wet strength additives for paper and reinforcement for polylactic acid (PLA) 3-D printing filaments. Our previous reports have attempted different approaches (e.g., direct esterification with organic acids and TEMPO-mediated oxidization) that render a modified fine with tunable functional groups for these applications. Some drawbacks of these approaches are noted below and alternative pathways have been utilized to control the surface chemistry of the lignin-rich fines.

The wet strength additives allow the formation of a physical polymeric network in paper under humid conditions.[2] For example, polyelectrolyte polymers such as polyamide amine epichlorohydrin can form ionic and ester bonds with pulp fibrils, resulting in an increased wet-tensile index by up to seven times. [3] The fines as wet strength additives can have a similar impact contributing to the bridging/densification of the fibril networks. However, these smaller particles may increase the resistance to dewatering.[1] This project aimed to study the reinforcement impacts of fine-based strength additives with a controllable amount of ionic groups (-COO-Na+). Our previous studies have utilized TEMPO-mediated oxidization route where 2,2 6,6 tetramethylpiperidine 1-oxyl (TEMPO) is used in conjunction with sodium hypochlorite and sodium bromide salt to oxidize primary hydroxyls into carboxylic acid groups (anionic COO-Na+). These COO- groups may help with the fine-based wet strength additives.[3] However, this method has low economic and reaction efficiency due to the side reaction; the oxidized reagents(e.g., NaClO) can degrade the lignin, changing (and solubilizing) their structure and consuming excessive amounts of reaction reagents. Beaumont et al. recently introduced a milder N-succinylimidazole route to selectively esterify the C6-OH groups forming a COOH by esterifying hydroxyls, while maintaining native structure and composition of the fiber.[4] This report applied this approach to modify fines and described its efficiency using Fourier transform infrared (FTIR) spectroscopy and microscopy. The untreated and modified fines were used as wet strength additives for handsheets (10 wt%). Their impacts were evaluated based on the subsequent handsheet characterization, including thickness measurements and horizontal tensile tests.

On the other hand, to fabricate fine/PLA composites, we need to address compatibility issues between the hydrophilic fiber and hydrophobic plastic. Incomplete mixing and lack of miscibility causes well-known phase separation in the matrix so that composite's strength and modulus decrease significantly. The substitution of primary hydroxyl groups with a long alkenyl chain was achieved using the above esterification route. Specifically, in place of succinic anhydride, dodecenyl succinic anhydride (DDSA) was selected to modify their surface hydroxyl groups for weakening the intramolecular hydrogen bonds, which will cause agglomeration in the PLA and organic solvent. Compared with our previous direct esterification approach with organic acid (oleic acid), the milder reaction conditions (room temperature) can reduce the cost and keep their native structure and composition. Furthermore, the enhanced dispersibility of the fines in hydrophobic solvents such as dichloromethane (DCM) and ethylene acetate (EA) also opens the door for initiating ring-opening polymerization of lactide monomers on the fine's surfaces. These modified fines potentially can be used as 3D printing inks.

Results

The fines were dispersed in acetone for surface modification. N-succinylation esterification was applied to convert the surface hydroxyl groups using imidazole as catalysts at 40 °C for 6.25 hrs. We chose succinic anhydride and glutaric anhydride to produce succinyl acid (SA) and glutaryl acid (GA) fines. The reaction efficiency was highlighted using FTIR spectroscopy (Figure 1). Modification was confirmed with peaks related to the newly form esters at 1740 cm^{-1} (COOH), 1590 cm^{-1} (C=O in ester), and 1170 cm^{-1} (C-O in ester). Our conductimetric titration analysis also shows that all three types of fines (fine, SA-Fine, and GA-Fine) possessed anionic COOH groups. Moreover, the modified fines demonstrated improved hydrophilicity as the fines were readily dispersed in water. These results indicated the successful addition of succinyl- and glutaryl- side chains on their surface. Currently, the fines are being analyzed for their total acid content using conductometric titration.

PROJECT 2.1

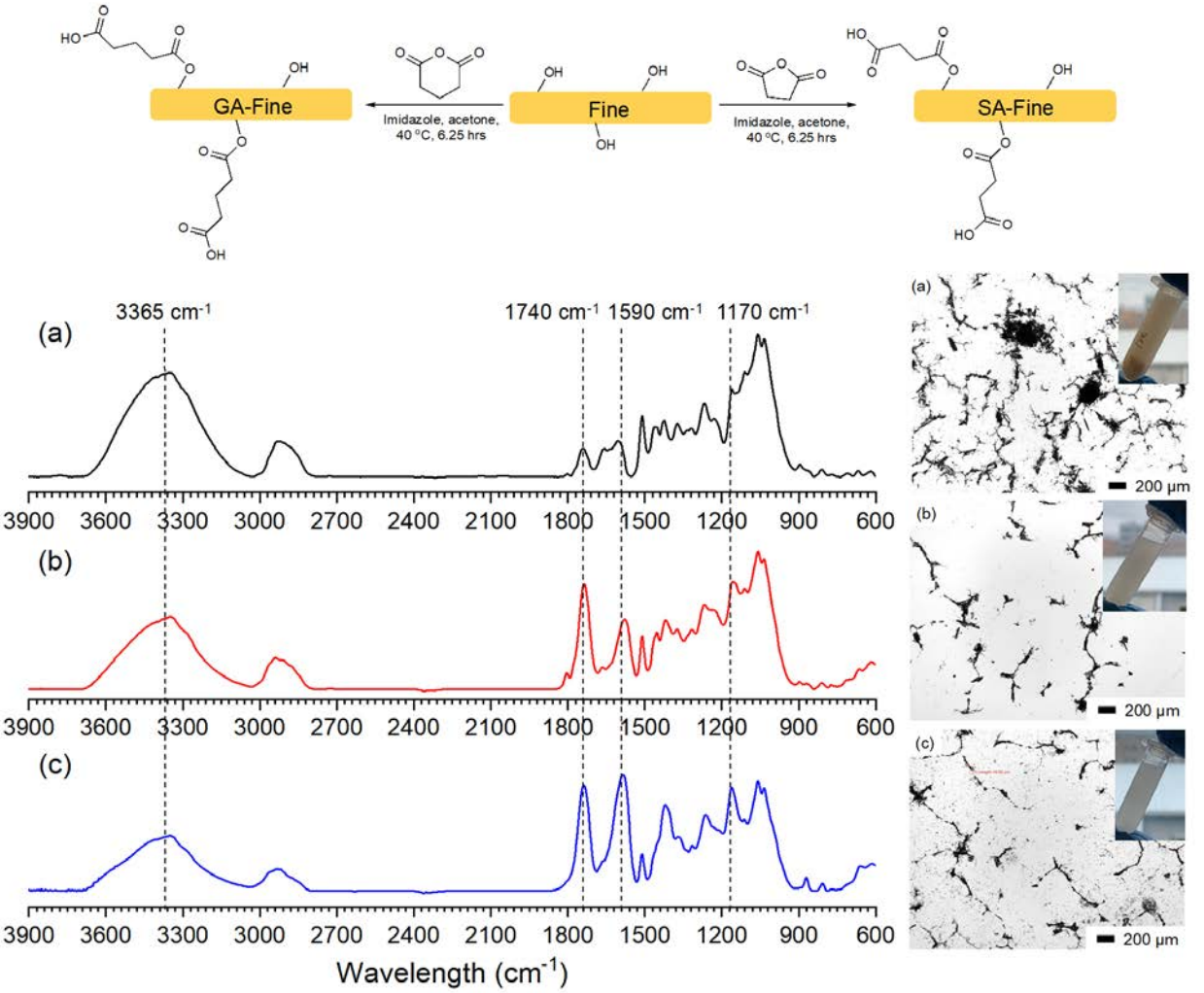

Figure 1 Reaction scheme (top) of the N-succinylimidazole esterification using glutaric anhydride and succinic anhydride; the FTIR spectra for (bottom left) of untreated fine (a), SA-fine (b), and GA-fine (c); the microscopy image (bottom right) of untreated fine (a), SA-fine (b), and GA-fine (c) and their dispersibility in the water.

These fines, as strength additives, were then added into handsheets (10 wt%) and the mechanical properties subsequently analyzed using the TMI horizontal tensile tester. As shown in Table 1, the fine-based additives can dramatically improve the mechanical performances of the handsheet, including tensile index (Tidx), elastic modulus (E-mod), and elongation at break. All values under the dry state have increased by 3% – 30% because of the reinforcing impacts of the fines. The wet tensile tests were performed by dipping the handsheets in the water for a few seconds and subsequently testing them. The additional fine content in the handsheet can increase their Tidx and E-mod by 37% - 85% because of the additional networks. Note that, the untreated fines also contain COOH groups (Figure 1). It may originate from hemicellulose or the oxidization of surface alcohol groups during the thermal heating process. Though SA-fines and GA-fines possess more anionic groups than untreated fines, the modified fine-based handsheets had lower Tidx, E-mod, and strain at break than fine-based handsheets. One reason is their smaller density. During the handsheet preparation, smaller fine particles (individualized anionic fines) may pass through the screen. We will then lose these hydrophilic fine additives in the handsheet. This loss then changes the density, thickness, and related tensile strength of handsheets. As a result, an appropriate retention aid is necessary (and will be applied) to keep these additives in the final handsheets. [5]

PROJECT 2.1

Table 1. The mechanical performances of fine containing handsheets.

	Grammage (g/m2)	Thickness (mm)	density (kg/m3)	Dry state			Wet state		
				Tidx [J/g]	E-mod [MPa]	Strain @break (%)	Tidx [J/g]	E-mod [MPa]	Strain @break (%)
HandSheet	69	0.14	510	24.56±2.58	2266±225.9	0.95±0.09	93.7±11.9	0.67±0.05	2.21±0.73
Fine-HS	58	0.12	504	31.35±1.55	2667±175.5	1.13±0.16	160.3±17.0	1.24±0.14	1.00±0.17
SAFine-HS	54	0.11	478	31.74±3.73	2693±305.9	1.04±0.08	127.7±8.4	1.07±0.06	1.03±0.10
GAFine-HS	55	0.11	483	30.53±2.52	2327±160.4	1.25±0.19	140.1±22.7	1.22±0.15	1.15±0.12

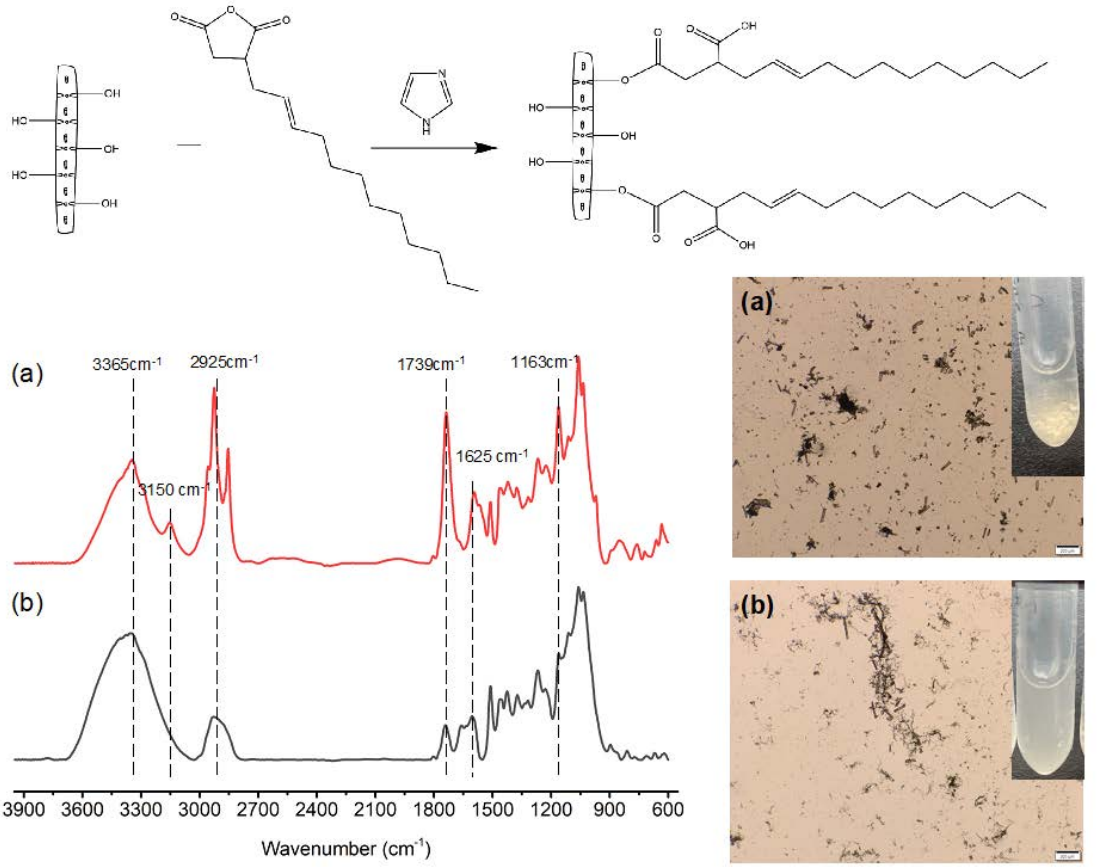

Figure 1 Reaction scheme (top) of the N-succinylimidazole esterification using 2-dodecen-1-ylsuccinic anhydride; the FTIR spectra (bottom left) of DDSA-fine (a) and untreated fine (b); the microscopy image (bottom right) of untreated fine (a), and DDSA-fine (b) and their dispersibilities in the ethyl acetate.

The above N-succinylimidazole modification route can also render the fine with more hydrophobic properties with the right reagent to improve their compatibility with the PLA. The wet fines were first dispersed in acetone. Dodecenyl succinic anhydride (DDSA) as reaction reagent was used with the imidazole as a catalyst to esterify hydroxyl groups at 40 °C for 6.25 hours.(Figure 2) A successful introduction of additional functional groups was determined by FTIR spectroscopy. (Figure 2) Compared with the unmodified fines, the long alkyl chains (C-H stretching) can be found around 2925 cm-1; the strong bands at around 1739 cm^{-1} (C=O in ester) and 1163 cm^{-1} (C-O in ester) also confirmed the presence of additional ester groups in the modified fines. In terms of the dispersion tests, the DDSA fines demonstrated increasing dispersibilities in hydrophobic solvents such as ethyl acetate and dichloromethane. Microscopy was used to show that the untreated fines tend to clump together with a size of 20 - 212 μm in ethyl acetate, while the DDSA fines have a smaller diameter (10 - 100 μm).

PROJECT 2.1

Further, we attempted to blend these fines with commercial PLA 3D-printing filaments using an extruder/compounder (180 °C for 10 min). Compared with the untreated fine, the DDSA-fine has improved compatibility with PLA illustrated with fewer clumps and more uniform filament diameter based on light microscopy imaging (Figure 3). As-is, there may be lower mechanical performances of these fine-based filaments attributed to a considerable amount of remaining fine agglomerations, causing a phase separation in the PLA filaments. To further address the compatibility issues, our future study will introduce modification using ring-opening polymerization with lactide. This process will result in grafting PLA from the fine surfaces.

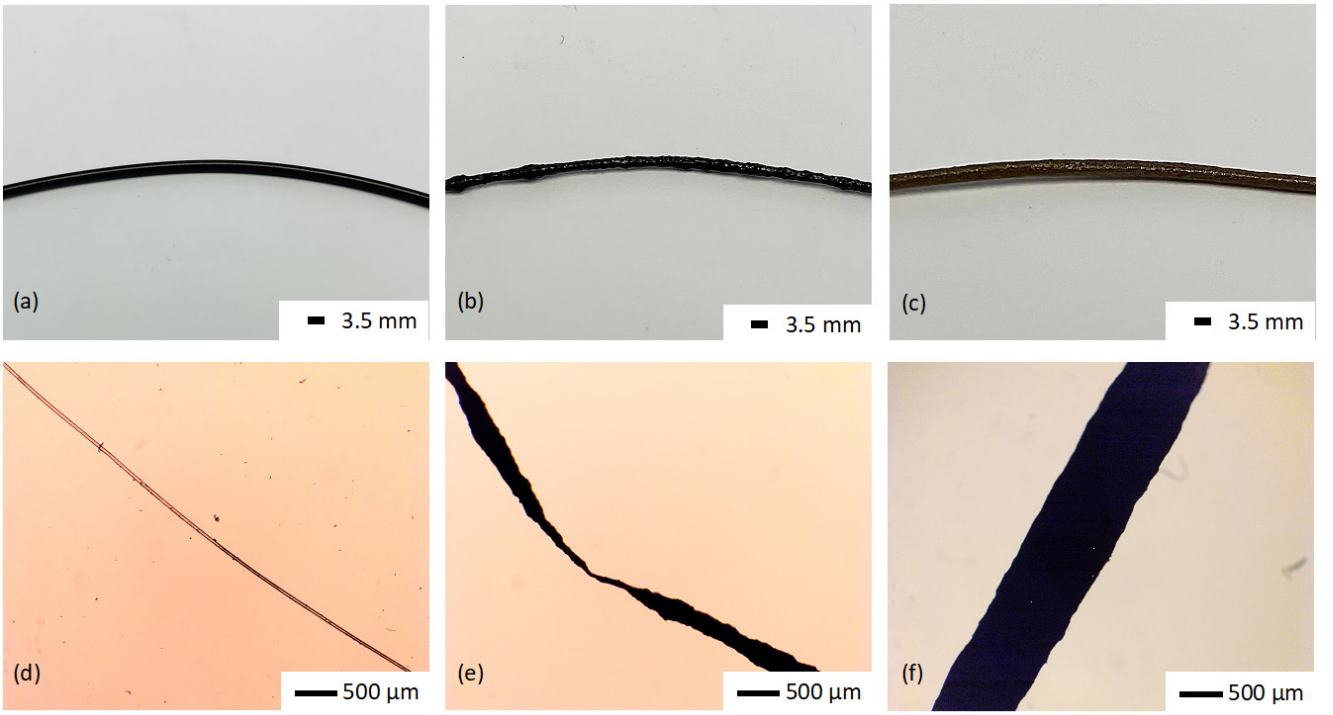

Figure 3 Images of PLA filaments without (a,d) or with fine addittices (b,e) and DDSA fine additives (c,f).

Future Research

The N-succinylimidazole esterification is an efficient route in adding different functional groups in the fine for both applications in this project. We successfully prepared anionic fines (containing COOH groups) by reacting the surface hydroxyl groups with the succinic anhydride and glutaric anhydride. When added to the hand sheets, these additives enhanced their dry and wet strength. However, the smaller particle size of modified fines requires retention aid (cationic polymers) to keep them in the handsheet. To optimize and understand the mechanism of fine-based wet strength additives, we plan to investigate effects such as the weight percentage of fine and the retention aids (e.g., cationic polymers) in our future work.

We can also add long alkyl chains on the fine's surface by applying the DDSA reagents through a similar modification method. The resulting DDSA fines have improved compatibility with PLA, as shown in their micromorphology. Further characterization of their mechanical performance is required to investigate the role of fine additives in these PLA filaments. Moreover, the DDSA fine with improved dispersibilities in ethyl acetate and dichloromethane allows the fine to initiate a ring-opening polymerization of lactide in fabricating PLA-fine copolymers. This "graft from" strategy can potentially tune the degree of polymerization for more advanced PLA/fine 3D printing inks in the future.

References

1. Odabas N, Henniges U, Potthast A, Rosenau T (2016) Cellulosic fines: Properties and effects. Prog Mater Sci 83:574–594.
2. Espy HH (1995) Mechanism of wet-strength development in paper: a review. Tappi J 78:90–99
3. Obokata T, Isogai A (2007) The mechanism of wet-strength development of cellulose sheets prepared with polyamideamine-epichlorohydrin (PAE) resin. Colloids Surface A Physicochem Eng Asp
4. Beaumont M, Tardy BL, Reyes G, et al (2021) Assembling Native Elementary Cellulose Nanofibrils via a Reversible and Regioselective Surface Functionalization. J Am Chem Soc 143:17040–17046.
5. Sanchez-Salvador JL, Balea A, Monte MC, et al (2020) Comparison Of Mechanical And Chemical Nanocellulose As Additives To Reinforce Recycled Cardboard. Sci Rep 10:1–14.

PROJECT 2.2

FROM TREES TO TREATMENT: FUNCTIONALIZING TMP EXTRACTIVES

Authors: Pierre Betu Kasangana, Cameron Zheng, Laurel Schafer, Heather Trajano

Background

Extractives such as terpenes have been used in the past as natural medicines.[1] The ability to modify their structures could create more potent therapeutics deriving from terpenes. Terpenes contain olefins, this provides opportunity for functionalization via hydroaminoalkylation using the catalysts developed by the Schafer group. Hydroaminoalkylation is a reaction which adds a C—H bond adjacent to the nitrogen atom of an amine across a double bond (or olefin).[2] Amination of β-pinene and limonene was previously demonstrated with our tantalum-catalyst using N-methylanline (NMA) (Fig. 1). We will use this catalyst to create aminated terpenoids.

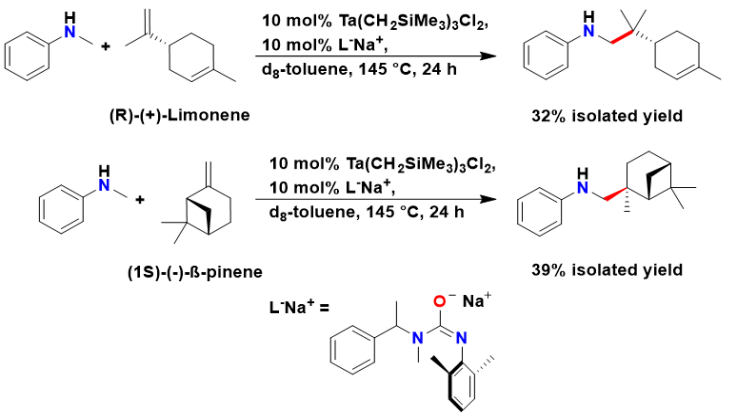

Figure 1. Reaction scheme for β-pinene and limonene amination by hydroaminoalkylation.[3]

Sub-project 1: Influence of fatty acids and resin acids on odour

In November 2021, we reported that we had detected fatty acids and resin acids in water streams throughout the mill environment during operations with aspen and softwood (white spruce and jack pine). Linoelic acid was found in the greatest concentration. Once released during pulping, linoleic acid and other fatty acids distribute between process waters and adsorption onto pulp surfaces. The adsorbed fatty acids persist through drying and remains with the market pulp. Once pulp is in transit, the fatty acids undergo auto-oxidation to odorous compounds such as hexanal and hexanoic acid. When pulp is used in food packaging, it must not introduce any unpleasant tastes or odours. Unfortunately, linoleic acid oxidation can occur at 20 to 50 °C.[4] Since November 2021, we have evaluated the effect of varying pH on the removal of linoleic acid from pulp.

Pulp (Meadow Lake Mechanical Pulp Inc.) was suspended in water of varying pH at 85°C for 10 minutes. After incubation, the water was recovered by filtration. A sample of filtrate was taken for chemical oxygen demand (COD) analysis.[5] Another filtrate sample was subjected to liquid-liquid extraction with hexane. A sample of the hexane extract was analyzed by GC-MS.

Results

Figure 2 presents the effect of pH on the desorption of linoleic acid from pulp. Maximum linoleic acid removal, as measured by GC-MS (Fig 2a), was observed for pH 6.5-7. The COD of the extracts was also measured (Fig 2b) and this analysis generally follows the same trend as GC-MS. Measurement of COD can serve as an indirect measure of troublesome extractives.

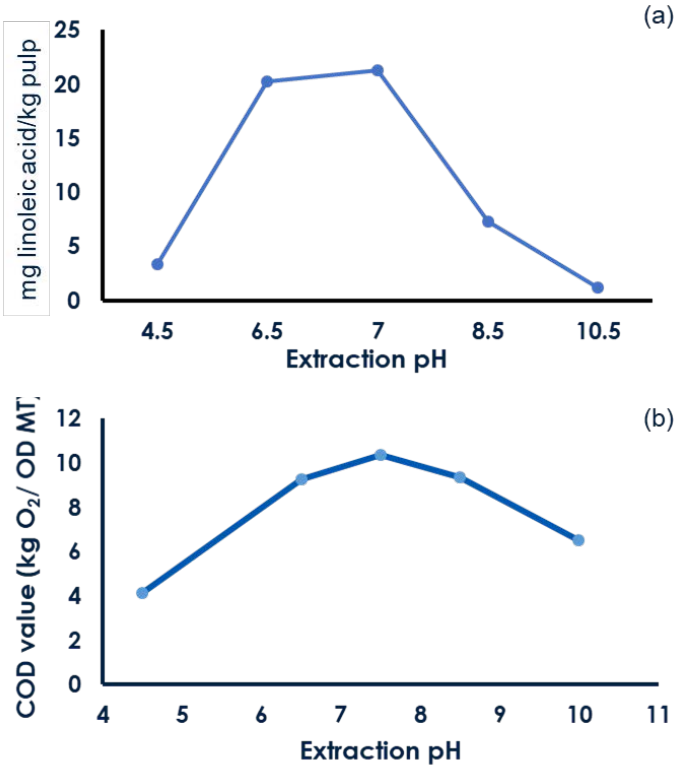

Figure 2. The effect of pH on extraction of linoleic acid from mechanical pulp derived from softwood (white spruce and jack pine). (a) Recovery of linoleic acid in the liquid phase as measured by GC-MS analysis. (b) The chemical oxygen demand (COD) of extract.

PROJECT 2.2

Sub-project 2: Catalytic transformation of terpenes

Catalytic upgrading of terpenes proceeded with 0.2 mmol each of N-methylaniline and extractive in 10 mol% of $Ta(CH_2SiMe_3)_3Cl_2$ and sodium ureate ligand dissolved in 0.3 mL d_8-toluene in a 1 dram vial. Afterwards, 0.33 equivalents of 1,3,5-trimethoxybenzene was added as internal standard. The homogenous solution was transferred to a J. Young NMR tube. After sealing the tube, an ^1H Nuclear Magnetic Resonance (NMR) spectrum was taken prior to heating. The J. Young NMR tube was then placed in heated in an oil bath (130 or 145 °C). After heating, ^1H NMR spectroscopy was used to determine terpene consumption.

Results

β-Myrcene is a monoterpenoid which can be extracted from Pine or Spruce resin, for example.[6] This extractive has reported antioxidant and anti-inflammatory properties.[6] These desirable properties inspired us to explore amination of β-myrcene to further enhance its positive bioactivity (Fig 3.). β-myrcene contains a terminal olefin and a geminal disubstituted olefin (together form a butadiene), and a trisubstituted olefins in its structure. From previous work, we expect with the terminal olefin functional group to react most readily with our catalyst.

An aminated terpenoid was generated with an NMR yield of 51%. An isolated yield of 17% was obtained and work is on-going to increase isolated yield. Through ^1H and ^{13}C NMR experiments, we were able to elucidate the structure of the product (Fig. 3). This structure reveals that our tantalum-catalyst produces the 1,4-addition product rather than the expected 1,2-addition product; such an addition was not known previously with this tantalum catalyst.

β-Caryophyllene is an example of a sesquiterpenoid which can be extracted from natural sources such as pine resin, oregano, black pepper, and Cannabis sativa.[7] This terpene is not only a flavour enhancer but has been proven to have positive effects when treating nervous system diseases and tumours.[7] Similar to β-myrcene, we subjected β-caryophyllene for hydroaminoalkylation with NMA (Fig. 4).

An aminated product was detected with a relatively high NMR yield of 76%. Work on obtaining a high isolated yield is on-going. As there is a geminal olefin and trisubstituted olefin in the structure of β-caryophyllene, we expected the geminal olefin to react for hydroaminoalkylation. Surprisingly, ^1H and ^{13}C NMR experiments revealed a product structure in which the trisubstituted olefin is reacted preferentially. The Schafer lab has not observed any cases where the higher substituted olefin reacted favorably since the disclosure of this catalytic system in 2019.[8]

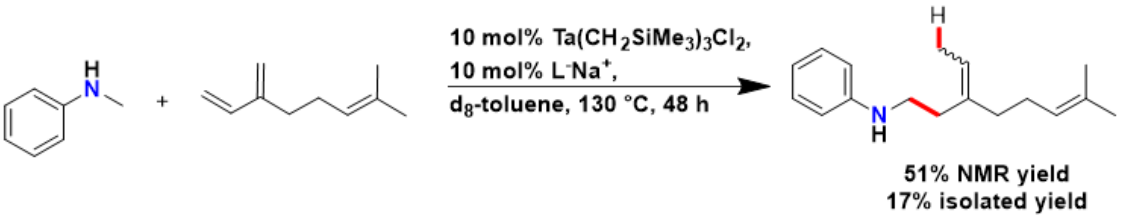

Figure 3. Hydroaminoalkylation reaction between β-myrcene and NMA

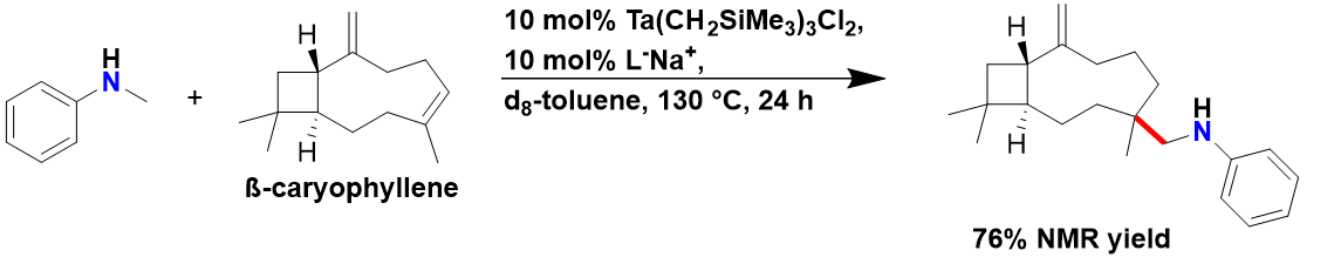

Figure 4. Hydroaminoalkylation reaction between β-caryophyllene and NMA

PROJECT 2.2

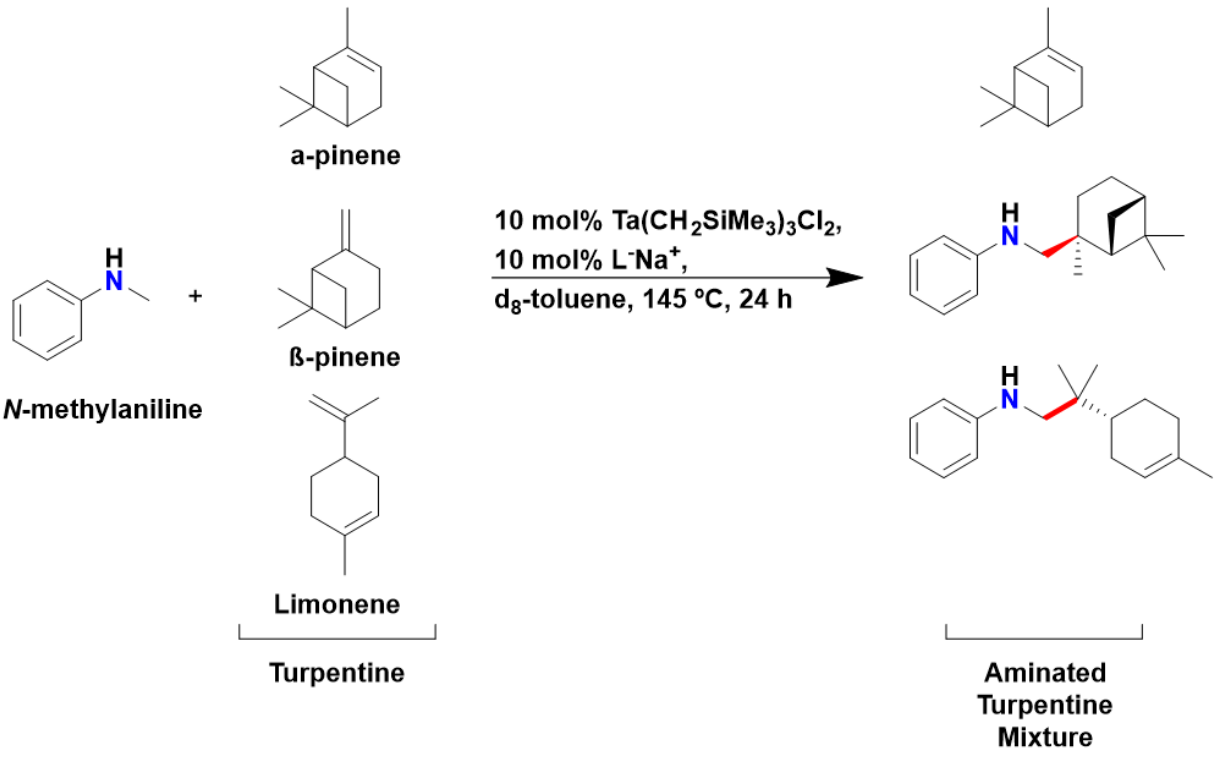

Figure 5. Reaction scheme for turpentine hydroaminoalkylation

Sub-project 3: Biological Screening

As reported previously, turpentine (Holmen Paper AB) was aminated using N-methylaniline at 145 °C for 24 hours (Fig. 5).

The biological activity of four samples was tested using the disk diffusion assay: **sample 1**: turpentine, **sample 2:** aminated turpentine, **sample 3:** turpentine treated with catalyst, and **sample 4:** N-methylaniline treated with catalyst. Literature findings disclosed that turpentine oil had anti-fungal activity against *Candidas cerevisiae* and anti-bacterial activity against *Escherichia coli.*[9] We anticipated that our aminated turpentine mixtures could enhance the existing anti-microbial properties of turpentine as amines are bioactive functional groups. We utilized *Candidas albicans* in our screening assay as it is pathogenic and phylogenetically similar to *C. cerevisiae.*

Reaction mixtures for **samples 2-4** were treated with pentane to remove catalyst by precipitation, filtered twice through Celite™, and pentane was removed by rotary evaporator. Positive controls were Nyastatin (commercial anti-fungal) and Rifampin (commercial anti-biotic). The solvent control was 0.5% dimethyl sulfoxide (DMSO) in distilled water. 40 µg/mL solutions in DMSO were made for **samples 1-4** and then diluted to 200 µg/mL in distilled water. 100 µL of each solution was absorbed onto cotton discs which were then placed onto a petri dish containing *Candidas ablicans* (fungus) or *Escherichia coli* (bacteria) on Mueller Hinton II agar. The petri dish was then incubated at 37 °C overnight to determine qualitative anti-microbial activity.

PROJECT 2.2

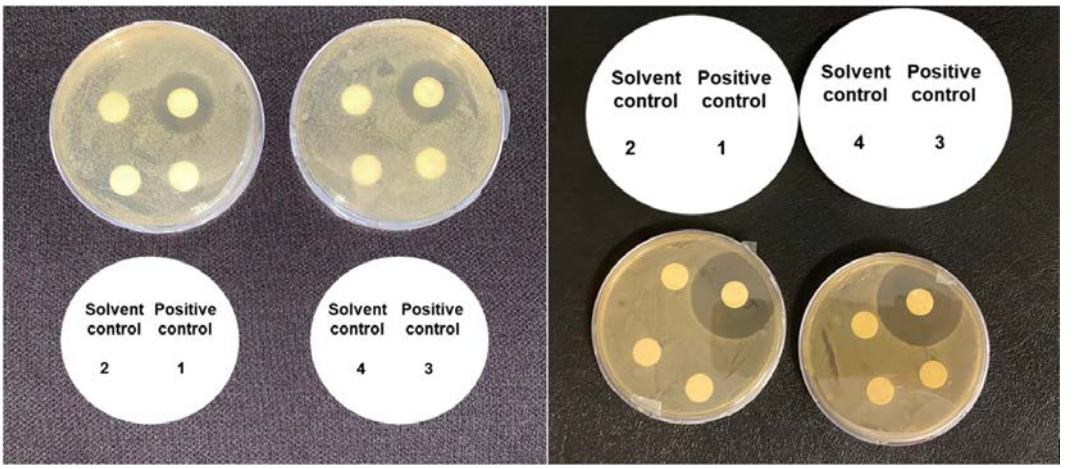

Figure. 6. Disk diffusion assay containing *C. albicans* (left) and *E. coli* (right). **Sample 1:** turpentine, **sample 2**: aminated turpentine, **sample 3**: turpentine treated with catalyst, and **sample 4:** N-methylaniline treated with catalyst. Solvent control was loaded onto the top left disc, and positive control was loaded on the top right disc.

Results

From our evaluation of turpentine and the aminated turpentine mixture, we do not observe any anti-fungal properties (Fig. 6). The amount of sample loaded onto each disc was as described in the literature for fungal growth inhibition. Similarly, we do not observe any bacterial growth inhibition for *E. coli* (Fig. 6).

Future Research

As we did not observe any anti-microbial activity as described in the literature, we will next screen against *C. cerevisiae* to confirm if the reported literature results are repeatable with our assay. Further, we desire to test our aminated β-myrcene and β-caryophyllene products for their bioactivity.

References

1. 1. Cox-Georgian, D.; Ramadoss, N.; Dona, C.; Basu, C. Med. Plants From Farm to Pharm. 2019, 333–359.
2. 2. Edwards, P. M.; Schafer, L. L. Chem. Commun. 2018, 54, 12543–12560.
3. 3. DiPucchio, R. C.; Rosca, S.; Athavan, G.; Schafer, L. L. ChemCatChem 2019, 11, 3871–3876.
4. 4. Pugh, S.; Guthrie, J.T. Cellulose. 2000, 7, 247-262.
5. 5. Boyles, W. The Science of Chemical Oxygen Demand Technical Information Series Booklet No. 9, USA: Hach Company, 1997.
6. 6. Surendran, S.; Qassadi, F.; Surendran, G.; Lilley, D.; Heinrich, M. Front. Nutr. 2021, 8, 400.
7. 7. Francomano, F.; Caruso, A.; Barbarossa, A.; Fazio, A.; Torre, C. La; Ceramella, J.; Mallamaci, R.; Saturnino, C.; Lacopetta, D.; Sinicropi, M. S. Appl. Sci. 2019, Vol. 9, Page 5420 2019, 9, 5420.
8. 8. DiPucchio, R. C.; Roşca, S.-C.; Schafer, L. L. Angew. Chemie Int. Ed. 2018, 57, 3469–3472.
9. 9. Schelz, Z.; Molnar, J.; Hohmann, J. Fitoterapia 2006, 77, 279–285.

PROJECT 2.3

MFC PRODUCTION, CHARACTERIZATION, AND PROPERTIES OF MECHANICAL PULPS

Authors: Mariana Frias de Albuquerque, Samira Gharehkhani, Rasmita Sahoo, James Olson, Boris Stoeber, Heather Trajano

Background

The present project aims to extend the utilization of short mechanical pulp fibres (L < 1.0 mm) toward the production of micro-fibrillated cellulose (MFC). Generally, we produce MFC through low-consistency (LC) refining. In this context, we employ fractionation and enzymatic treatments to reduce MFC production energy and alter MFC characteristics. We investigate MFC properties through characterization methods such as rheology and visualization through scanning electron microscopy (SEM) and micro-computed tomography scanning (micro-CT).

Since November 2021, we have focused on the rheology of MFC, and the enzymatic pre-treatment of the mechanical pulp fibres. We have prepared a journal manuscript on our previous study of MFC as a reinforcement agent.

Sub-project 1: Incorporating selective fibre fractionation with MFC production to create high bulk-tensile paper

There is a desire for future mechanical pulp materials that are suitable for packaging as well as absorbency grade paper that is porous and thick (high bulk) with sufficient (minimal) strength for particular applications [Ghose et al. 2013]. In the present work, we fractionate the whole pulp employing a pressure screen with either 0.5 mm sized holes (screen A) or 0.8 mm holes (screen B). The accept stream with the short fibre fraction is LC refined at different specific refining energies (SRE). It is notable that the short fibres refined at the highest SRE (896 kWh/t for pulp A, 1059 kWh/t for pulp B) are considered MFC-like materials. The refined short fibres are then blended with the reject stream to form and characterize handsheets. For comparison, whole pulp is also refined to equivalent SRE. Our results will shed light on the application of cost-effective MFC in packaging, absorbency grades and other products.

The initial fibre length of unfractionated pulp, accept A, accept B, reject A, and reject B are 1.6 mm, 0.8 mm, 1 mm, 1.8 mm, and 1.89 mm, respectively. Figs. 1 (a & b) shows the bulk as a function of SRE and tensile index, respectively, for all composites. In Fig. 1a, a reduction in bulk versus refining energy is observed for all fibre composites except the composite containing 8% accept fibres. In this case, the fines may not be well-retained in the porous open sheet structure when there is limited accept pulp. In general, the composites show a wide range of bulk corresponding to various paper grades from tissue paper to corrugated grade and catalog grade paper, which suggests that the combination of refined short fibres and long fibres is a versatile approach to manufacturing various paper grades.

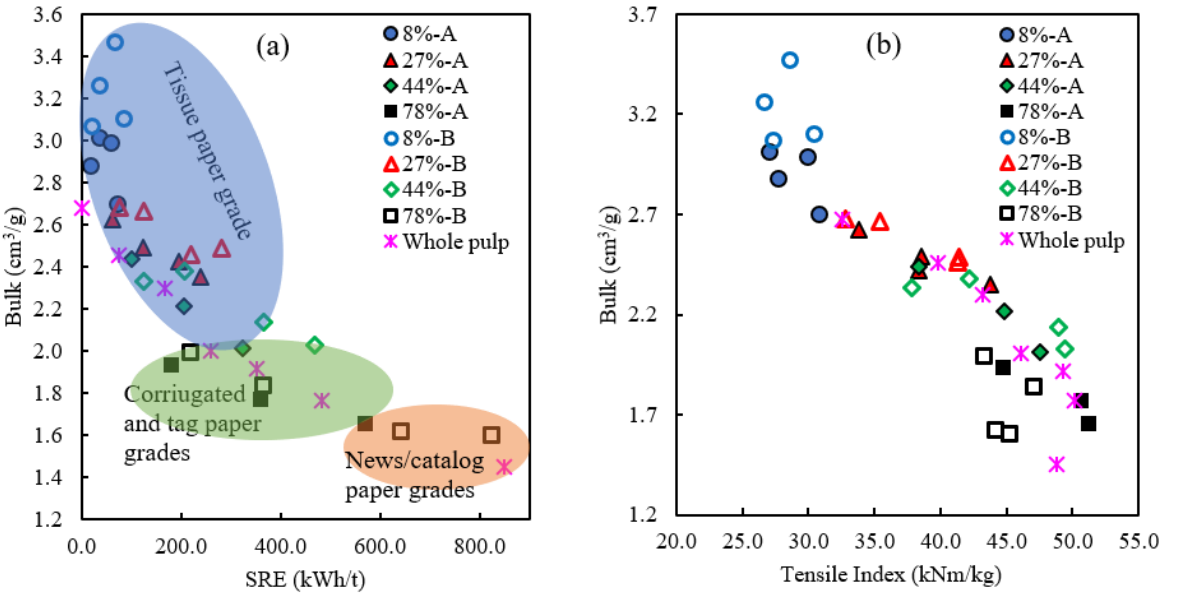

Figure 1. Relationship of a) bulk-SRE, b) bulk-tensile index for all composites; the percentage indicates the accept (short fibre) fraction in the composite

PROJECT 2.3

In Fig. 1b, it is observed that a small amount of SRE applied to the accept fibres largely preserves bulk while increasing the tensile index. The results also demonstrate that at a given bulk, the tensile index is more developed when the accept fibres are refined to the point of an MFC-like material and mixed with the reject fibres at a ratio corresponding to the mass reject ratio (27% for screen A and 44% for screen B). The composites consisting of 78% refined accept fibres have the lowest bulk compared to the whole pulp and the other composites at the same SRE due to the shortest average fibre length.

Fig. 2 shows a decrease in tensile energy absorption (TEA) with bulk. At a given bulk, almost all composite samples show higher TEA than the whole pulp, revealing that the presence of refined accept fibres increases the ability of the composites to withstand stress and rupture.

Fractionation, selective chemical or enzymatic treatment, and refining of the accept pulp reduces the required SRE while increasing strength. This approach has the advantage of only requiring treatment of a small percentage of the pulp.

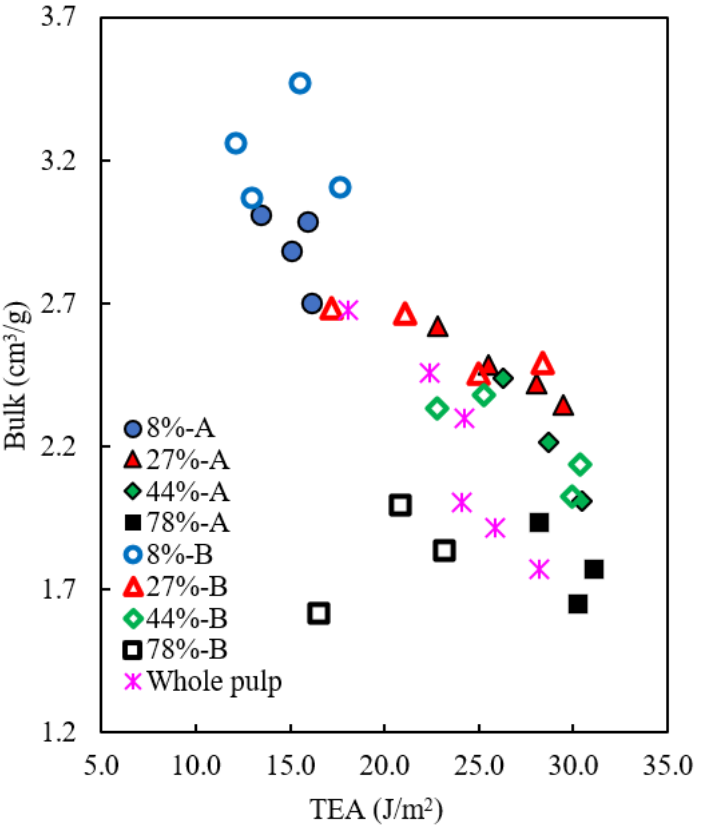

Figure 2. Relationship of bulk-TEA for all composites

Sub-project 2: The dynamics of flocs formulated by MFC suspension under shear

Our aim is to understand how the degree of fibrillation affects the suspension rheology of MFC. However, the high aspect ratio of fibres and strong inter-fibrillar forces make it challenging to assess complex rheological properties using conventional rheometers.

Rheological experiments are performed on suspensions of short fibres (screen B) prepared with different SRE. Fibre suspension consistency was varied but only results generated at 1 wt% consistency are reported here. A Kinexus rheometer with 40 mm diameter parallel plates was used to to determine flow curves and visco-elastic properties. Preliminary rheological measurements suggest that fibres under shear migrate away from the wall creating a lubrication layer and wall slip. Hence, sand paper was attached to parallel plates to prevent wall slip.

Results

The shear rate dependent viscosity of fibre suspensions at 1% consistency is shown in Figure 3. At low shear rate, the viscosity increases with refining energy, while all suspensions show shear-thinning behaviour. At the intermediate shear rate (0.1-1 s^{-1}), the viscosity curve shows shear thickening behaviour; here shear-induced flocculation occurs as shown in the image (the end of a floc shows at the edge of the parallel plate geometry). Fibre flocs form aligned in the vorticity direction. At a high shear rate, those flocs appear to disintegrate leading to shear-thinning behaviour.

The fibre suspensions were exposed to a constant shear rate 0.8s^{-1} for 15 mins and the shear-induced flocs were observed by lifting the upper plate as shown in Figure 4. The flocs formed by unrefined short fibres are long and well-defined (Figure 4(b)) while the flocs formed by MFC-like material (991 kWh/ton SRE) are shorter and less distinct.

Figure 5 shows the angular frequency dependent storage modulus (G') and loss modulus (G") for 1 wt% fibre suspensions. The suspension elasticity increases significantly with SRE. This is most likely associated with a more interconnected fibre network due to increased fibrillation.

This pronounced viscoelastic properties of MFC can be related to the morphology of the flocs in Figure 4(d). These results show that the degree of fibrillation is reflected in the rheological characteristics of the fibre suspensions. However, further studies are required to identify the most suitable rheological measure.

PROJECT 2.3

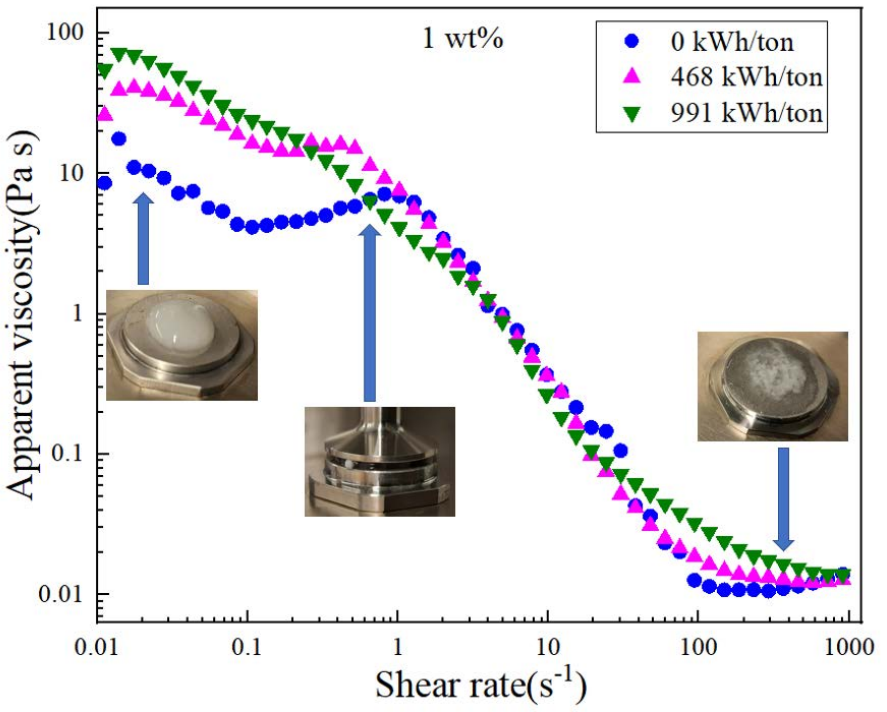

Figure 3. Relationship of bulk-TEA for all composites

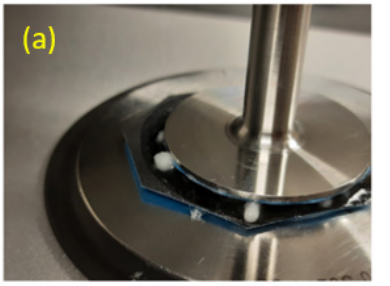

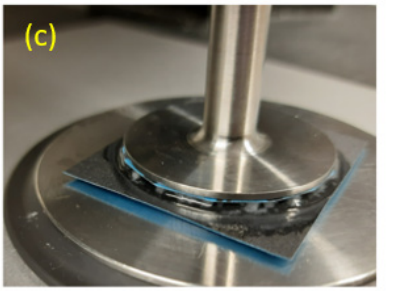

Figure 4. Formation of flocs after constant shear at 0.8 s-1 for 15 minutes. Suspension consistency was 1 wt%: (a), (b) Unrefined short fibres (0 kWh/ton SRE); (c), (d) MFC-like material (991 kWh/ton SRE).

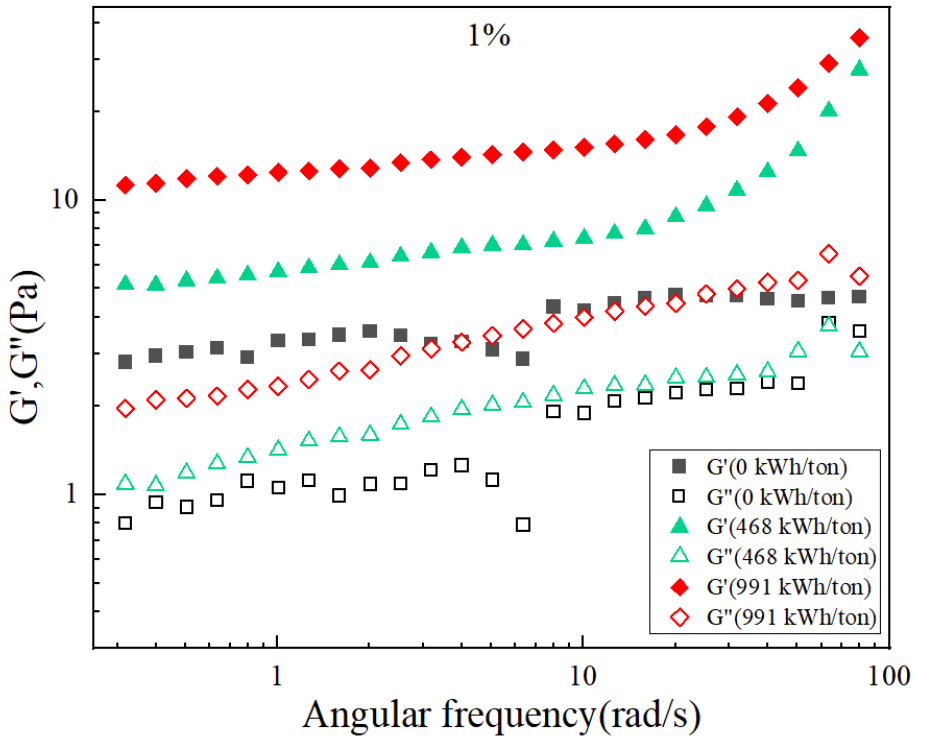

Figure 5. Angular frequency dependent storage modulus (G') and loss modulus (G") at a constant shear strain 0.5% for fibre suspensions (1 wt% consistency) with different levels of SRE.

PROJECT 2.3

Sub-project 3: The effect of enzyme hydrolysis on refining mechanical pulp fibres

Previous research on Kraft pulp shows that it is possible to reduce energy requirements for MFC production by treating fibres with enzymes such as cellulase prior to refining (Henriksson et al., 2007). Endoglucanase is the most common enzyme used for MFC production; its primary function is to act on internal sites of cellulose chains. Other enzyme types, exoglucanase, xylanase, and mannanase, have distinct functionalities and have been shown to potentially change the evolution of fibre morphology. The interaction of enzymes and refining on MFC properties is still not well established, particularly when using mechanical pulp. Thus, this sub-project aims to combine enzymatic pretreatment and refining of mechanical pulp fibres and evaluate their effect on fibre morphology.

Short fibres (screen B) were subjected to hydrolysis with different enzyme species (Table 1) and then refined in a PFI refiner. Length and fines content of the treated fibres was measured using the Fibre Quality Analyzer (FQA). The experimental conditions are listed in Table 2. For the endoglucanase + exoglucanase + mannanase combination, the endoglucanase dosage was 0.5 or 5 % OD w/w; exoglucanase and mannanase were added as auxiliary enzymes at 10% w/w of endoglucanase.

Table 1. Enzyme species and combinations used in sub-project 3.

Enzyme species			
Control group: Refining only	Endoglucanase	Exoglucanase	Endoglucanase + Exoglucanase + Mannanase

Table 2. Experimental conditions of the initial stage of sub-project 3 to analyze the effect of dosage and refining level on fibre morphology.

Consistency (%)	Incubation Temperature (°C)	Incubation pH	Incubation Time (h)	Enzyme Dosage (% OD w/w)	PFI Refining Level (revolutions)
3.5	60	6	2	0.5	5,000
				5	20,000

Results

Figure 6 presents the effect of different enzyme treatments at varying dosage and refining level on average fibre length reduction. The effect of additional enzyme species will be presented at the Steering Committee Meeting.

The addition of an enzymatic treatment prior to refining facilitates the refining action, leading to a reduced fibre length. As expected, a higher level of refining results in more significant fibre length reduction for all systems.

It is also interesting to observe that, when combining the action of endoglucanase, exoglucanase and mannanase at 20,000 PFI revolutions, fibre length is reduced by about 24% with only 0.5% enzyme dosage. The same length reduction is achieved at 5% endoglucanase after refining at the same refining level. This indicates that it is possible to obtain more refined fibres with lower doses of enzyme treatment. Further investigations will be carried out in order to assess the degree of fibrillation of the fibres produced.

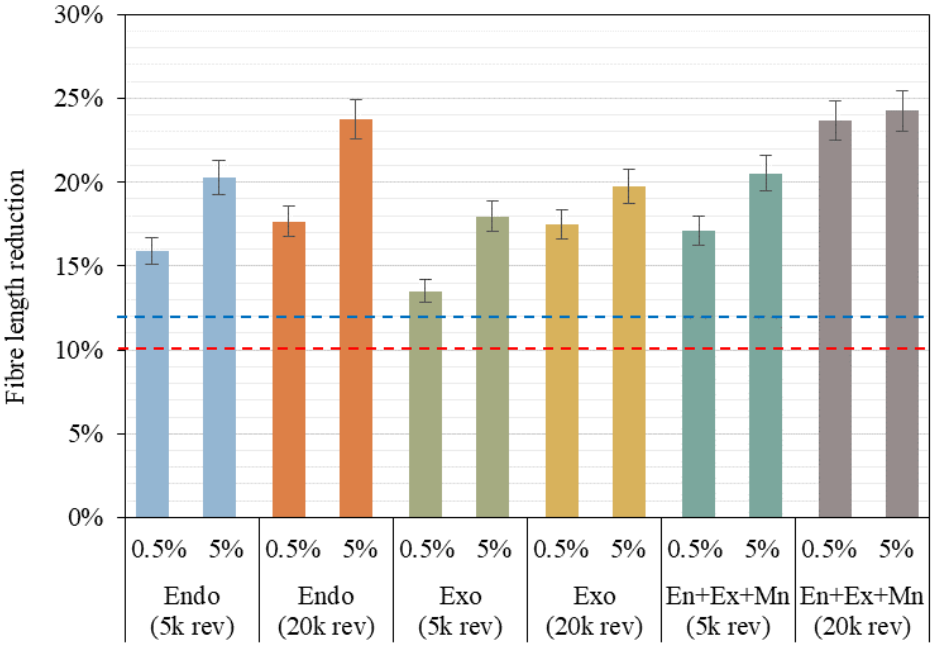

Figure 6. Effect of enzyme dosage and refining level on fibre length reduction, relative to untreated fibres, measured by FQA. The red dashed line indicates the result of refining at 5,000 revolutions, and the blue dashed line indicates refining at 20,000 revolutions, both without enzymatic hydrolysis.

PROJECT 2.3

Future Research

We will extend our work toward film and coating applications. MFC films with tailored optical characteristics will be made. The application of MFC as a coating material will also be examined. To get an even distribution of MFC on the paper surface, a proper formulation of MFC suspension needs to be developed.

The flow behaviour of fibre suspensions can not be fully understood from bulk properties alone. The formation of those flocs may create concentration gradients or a fibre free lubrication layer near the wall. To better understand the suspension behaviour for different degrees of fibrillation we plan to visualize the suspension microstructures under different flow conditions. Optical coherence tomography (OCT) may be a suitable tool for these visualizations.

In order to better understand the influence of enzyme action and refining on fibre morphology, we will perform a systematic study of the enzymatic hydrolysis process. We aim to evaluate the effect of incubation temperature and pH on the treatment.

Furthermore, we will combine FQA with imaging to visualize the fibres, and we will quantify fibrillation with the crill method. The latter consists of "a technique for qualitatively assessing loose slender and fibrillar particles created during pulping" (Osong et al, 2014). Recently, it was reported that the results of crill method can also be directly related to handsheet properties (Ekbåge et al, 2020). Finally, handsheets and coatings will be formed from the treated fibres in order to relate enzymatic hydrolysis parameters and paper properties.

References

1. Ekbåge, D., Nilsson, L., Håkansson, H., & Lin, P. I. (2020). Multiple linear regression modelling of pulp and handsheet properties based on fiber morphology measurements and process data. BioResources, 15(1), 654-676.
2. Ghose, A., & Chinga-Carrasco, G. (2013) Environmental aspects of norwegian production of pulp fibres and printing paper. Journal of Cleaner Production 57: 293-301.
3. Henriksson, M., Henriksson, G., Berglund, L. A., & Lindström, T. (2007). An environmentally friendly method for enzyme-assisted preparation of microfibrillated cellulose (MFC) nanofibers. European polymer journal, 43(8), 3434-3441.
4. Karppinen, A., Saarinen, T., Salmela, J., Laukkanen, A., Nuopponen, M. and Seppala, J. (2012). Flocculation of microfibrillated cellulose in shear flow. Cellulose 19: 1807-1819.
5. Osong, S. H., Norgren, S., Engstrand, P., Lundberg, M., & Hansen, P. (2014). Crill: A novel technique to characterize nano-ligno-cellulose. Nordic Pulp & Paper Research Journal, 29(2), 190-194.
6. Shafiei-Sabet, S., Martinez, M. and Olson, J. (2016). Shear rheology of micro-fibrillar cellulose aqueous suspensions. Cellulose 23: 2943-2953.
7. Haavisto, S., Salmela, J., Jasberg, A., Saarinen, T., Karppinen, A. and Koponen, A. (2015). Rheological characterisation of microfibrillated cellulose suspension using optical coherence tomography. Tappi Journal 291

On the right side, an optical microscopy image of enzyme-treated BCTMP fibres at 0.5% enzyme dosage using a combination of endoglucanases, exoglucanases and mannanases, plus refining at 20,000 PFI revolutions. **Author: Mariana Frias de Albuquerque, Ph.D. student.**

PROJECT 3.1

CREATING BULKY FIBRES

Authors: Elisa Ferreira, Anderson Veiga, James Drummond, Emily Cranston, Mark Martinez

Background

Paper properties such as absorbency, bulk and tensile strength are linked to fibre structure and surface chemistry. This project aims to create products from mechanical pulps with high bulk and high tensile index by applying surface modification in fibres. The proposal is to prevent fibre collapse by controlling the interfacial tension inside the lumen with hydrophobic surface functionalization and/or reinforce the fibre cell wall with chemical cross-linking. For characterizing fibre and paper products with several surface chemistries, we are developing tools to characterize fibre morphology by computed X-ray tomographic microscopy (μCT)

As porous carbon materials cannot attenuate X-rays efficiently, μCT images of fibres have low contrast, providing limited information for 3D-visualization. Here, we are developing methods to label fibres with metals that exhibit high X-ray attenuation, which potentially will improve fibre visualization by μCT. Our previous results showed that iron oxide nanoparticles can be formed in situ on the surface of CTMP (chemical thermomechanical pulp) fibres, forming a uniform particle layer, which generated a high contrast in μCT images. A similar approach was previously demonstrated with cellulose nanofibers and fibre fragments labelled with $CoFe_2O_4$ nanoparticles; however, the method was not efficient in applying metal nanoparticles on fibres (Hobisch et al., 2021).

In the current work, we show that a continuous iron oxide layer can be applied on CTMP through multiple labelling steps. The high iron content on fibre surface will potentially enhance the contrast for visualization by μCT. Finally, we demonstrate that the labelling method can be applied to analyse liquid dynamics on paper by producing iron nanoparticles in situ as tracers for liquid flow. Current paper research indicates that liquid flow through paper can be described by two liquid fronts and models to describe fluid mechanics are under development (MacDonald, 2018; Kvick et al., 2017; Bico & Quéré, 2003). As understanding liquid dynamics in paper is key to tailoring absorbency in paper products, we introduced tracers to reveal wetting fronts in paper and cellulose materials.

Experimental work

Fe-labelling. CTMP long fibres (length ~ 3.5 mm) were dispersed at 0.1% consistency in a solution of 0.18 mol/L $FeSO_4$ at 90 °C for 3 h. After soaking the fibres, the supernatant was removed, and the fibres were re-dispersed in water. A solution of NaOH was added into the flask at a final concentration of 0.54 mol/L and system was kept at 90 °C for 3 h to induce precipitation of iron oxide nanoparticles. After the precipitation, fibres were rinsed with water until neutral pH and clear supernatant. The procedure was repeated up to four times (i.e., multiple precipitation steps). After labelling, fibres were oven-dried at 60°C for 24 h. Fibres and handsheets (with unlabelled and with 100% labelled fibres) were characterized.

Liquid dynamics on paper. Filter paper strips (3 cm wide, 7 cm long) were immersed in a $FeSO_4$ aqueous solution and freeze-dried. After this impregnation with iron ions, the paper strips were partially immersed in a reservoir containing NaOH aqueous solution. The rise of the liquid front (NaOH solution) up the paper was tracked by the precipitation of iron oxide nanoparticles. Finally, samples were rinsed with water to remove unreacted iron ions.

Results

Multiple steps of Fe-labelling on CTMP fibres

The Fe-labelling method was designed for in situ preparation of iron oxide nanoparticles on fibre surfaces, by two steps: (1) impregnation of iron ions on the surface of the fibres, and (2) precipitation of iron oxides nanoparticles by increasing the pH with NaOH solution. Fe-labelled fibres exhibited a black color and, after rinsing with water, the nanoparticles remained attached to the fibre surface, indicating that the nanoparticles were strongly attached to the fibres (Figure 1).

Morphological analysis by polarized optical microscopy (POM) and scanning electron microscopy (SEM) revealed the formation of a robust coating of iron oxide (Fe_3O_4) nanoparticles on the fibre surface (Figures 1b.2-3) and a continuous layer after four labelling steps (Figures 1c.2-3). The inorganic content increased from 3 wt% (unlabelled fibres) to 54 wt% after four precipitation steps, as determined by thermogravimetric analysis. Since the nanoparticles are irreversibly attached to the fibres, Fe-labelled fibres are enabled for analysis of micro-mechanical behaviour and water absorption in paper products and show improved contrast in μCT (Figure 2).

PROJECT 3.1

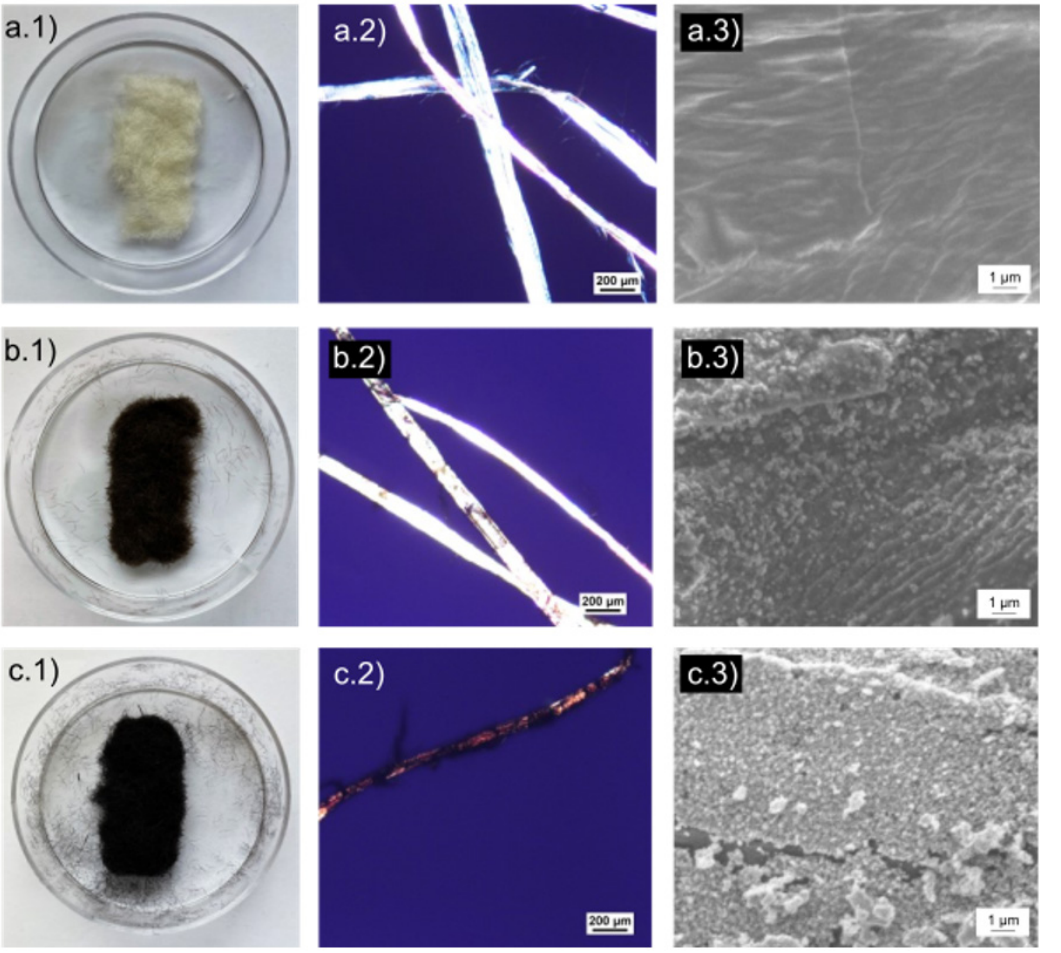

Figure 1. Images of CTMP fibres: (a) unlabelled (control), Fe-labelled fibres after (b) one and (c) four labelling steps. (a-c.1) Macroscopic view, (a-c.2) POM, and (a-c.3) SEM images showing a zoomed in area on a fibre.

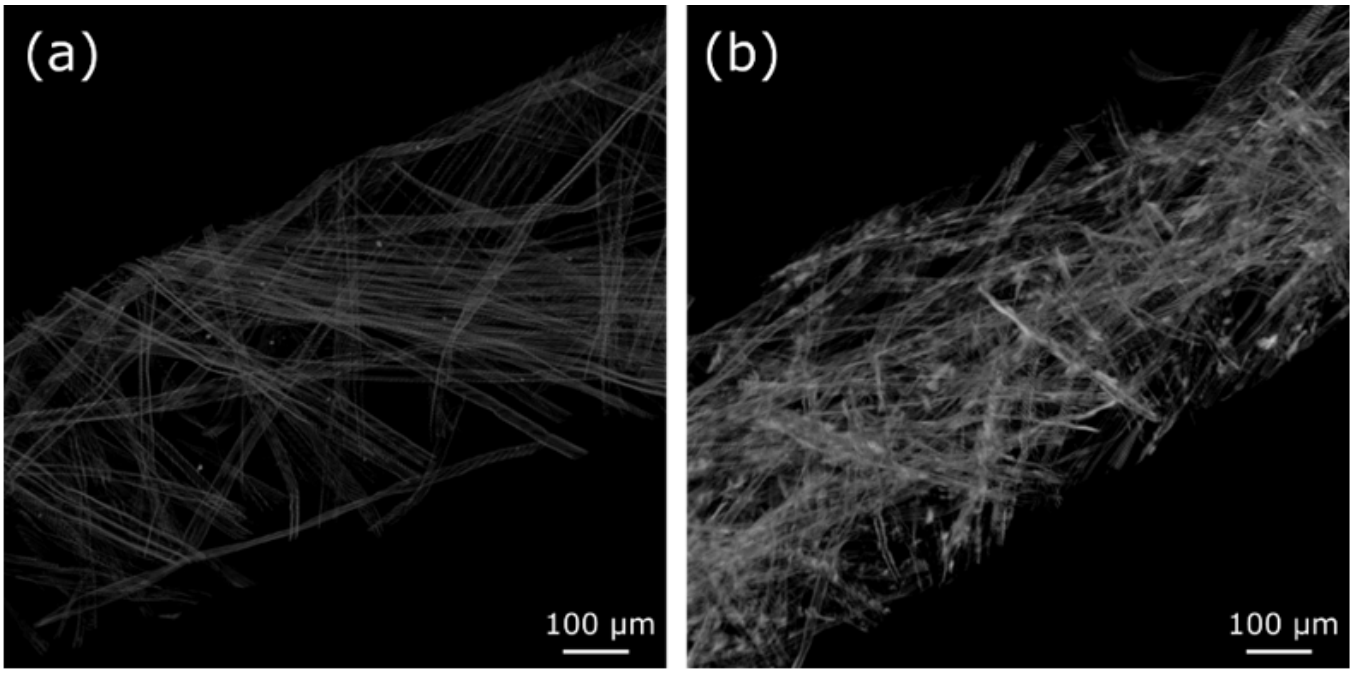

Figure 2. 3D reconstructed µCT image of a paper handsheet prepared with (a) unlabelled, (b) Fe-labelled fibres. The analysis reveled that Fe particles distributed through the sample enhance the contrast for fibre visualisation.

PROJECT 3.1

Liquid dynamics in paper

The Fe-labelling method was applied to analyse liquid dynamics in paper by precipitating iron oxide nanoparticles with a NaOH solution as the liquid front. After the test (Figure 3), the paper samples exhibited three regions: (i) a dark orange bottom area that had been immersed in NaOH solution; (ii) a light orange area that was wet by the NaOH solution through capillary flow; (iii) a white top area that had no contact with the NaOH solution (Figures 3b-d). SEM analysis showed the formation of iron oxide nanoparticles in regions (i) and (ii), successfully marking areas that were imbedded in NaOH solution and areas reached by the liquid front (Figures 3e-g).

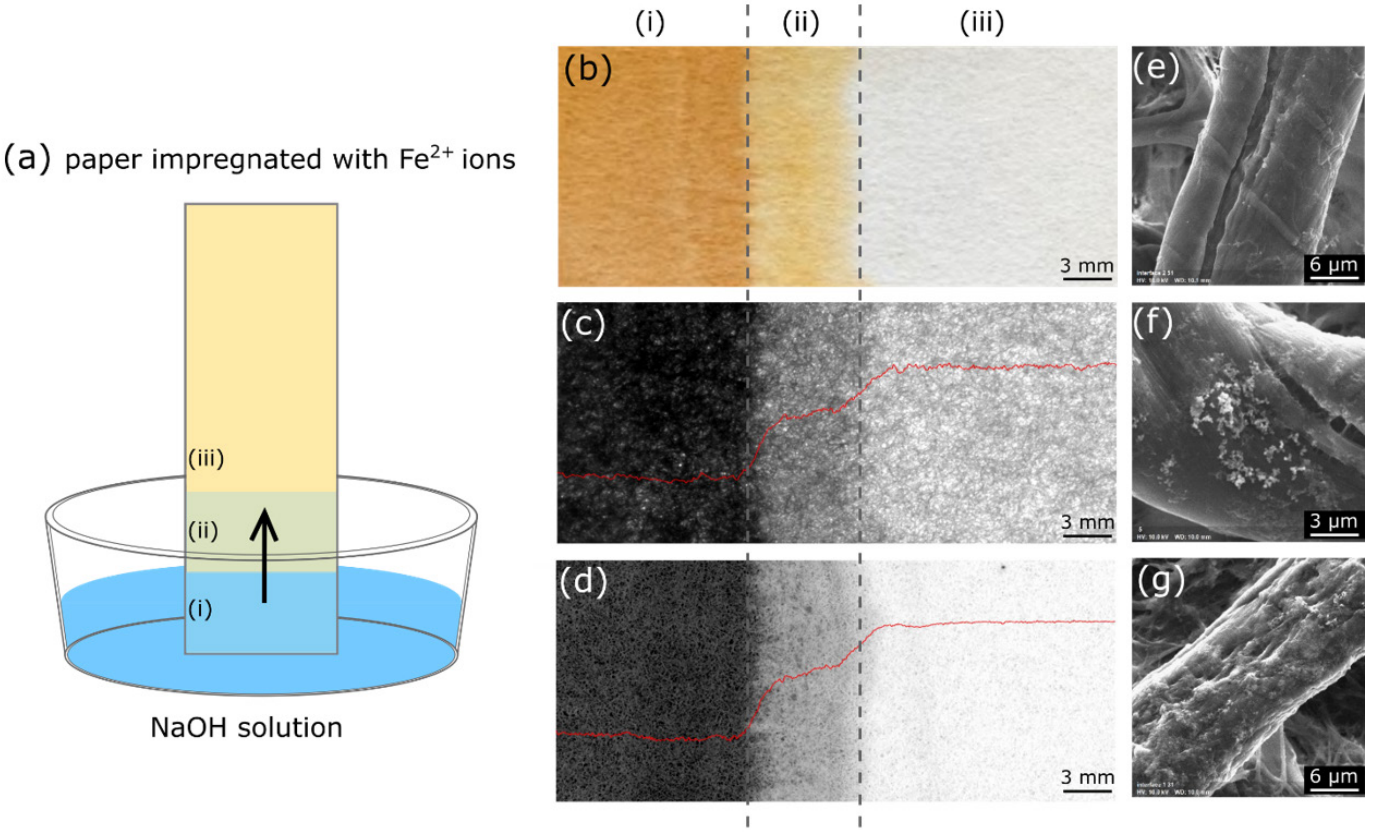

Figure 3. Liquid flow through paper as revealed by iron oxide nanoparticles, showing three regions: (i) nanoparticles precipitated on fibres by immersion in NaOH solution; (2) nanoparticles precipitated by the liquid front (NaOH solution), (iii) fibres with no contact with NaOH solution. (a) schematic representation of the test; (b) macroscopic view of paper strip with iron oxide nanoparticles; (c) image from transmitted light; (d) image from reflected light. Red curves represent the average grey scale at each region. SEM images from fibres in the regions: (e) i; (f) ii; and (g) iii.

Future Research

In the next steps, Fe-labelled fibres will be added in paper handsheets as tracers for fibre visualization by µCT analysis. Paper handsheets will be prepared within a range of tracer content to investigate suitable conditions for image analysis with minimum impact on paper properties. Ultimately, we will apply Fe-labelling to characterize the structure, mechanical properties and dynamics in water of bulky fibres by in situ testing coupled with µCT.

References

1. Bico, J., & Quéré, D. Precursors of impregnation. Europhys. Lett (2003), 61 (3).
2. Kvick, M., Martinez, M., Hewitt, D. R., & Balmforth, N. J. Imbibition with swelling: Capillary rise in thin deformable porous media. Physical Review Fluids (2017), 2(7), 074001.
3. Hobisch, M. A.; Zabler, S.; Bardet, S. M. et al. How cellulose nanofibrils and cellulose microparticles impact paper strength—A visualization approach. Carbohydr. Polym. (2021), 254, 117406.
4. MacDonald, B. D. Flow of liquids through paper. Journal of Fluid Mechanics (2018), 852, 1.

PROJECT 3.2

ADVANCED CHARACTERIZATION – COMPUTED TOMOGRAPHY

Authors: Aurélien Sibellas, Samuel Brown, James Drummond, André Phillion, Mark Martinez

Background

This project supports most of the other projects in this consortium through development of advanced quantitative microscopy. In the previous reporting period, we reported successful development of imaging protocols to acquire high resolution images of both papers made from mechanical pulps and of wood chips. We were also able to develop protocols to image deformation of wood and paper in uniaxial compression and tension. Building on this, during this reporting period, we have focussed on developing image quantification tools and have applied these to understand:

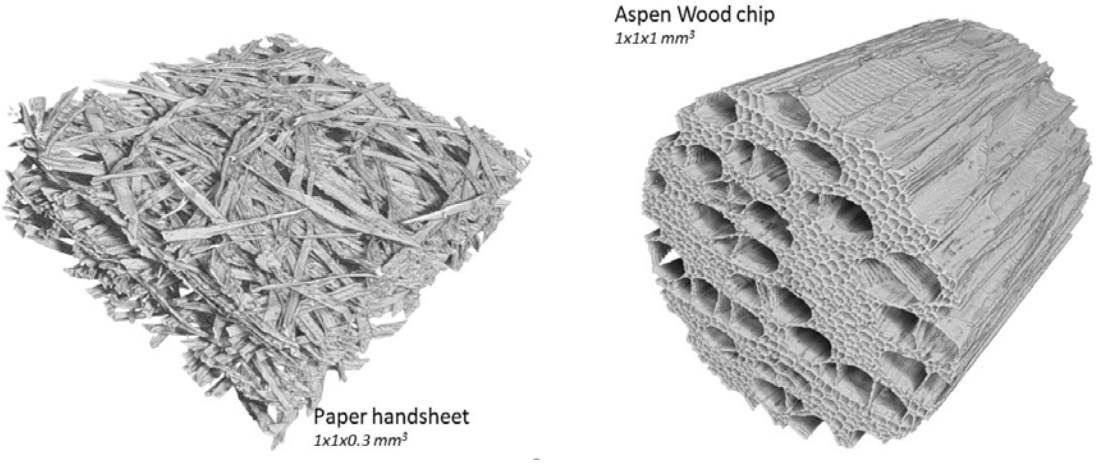

a. Strength development in paper by developing algorithms to quantify the number of contacts in fiber networks

b. Chip impregnation by measuring swelling of the fibre wall as a function of chemical treatments

c. Bulk preservation by developing algorithms to characterize wall damage and fibre collapse during compressive loading

Results

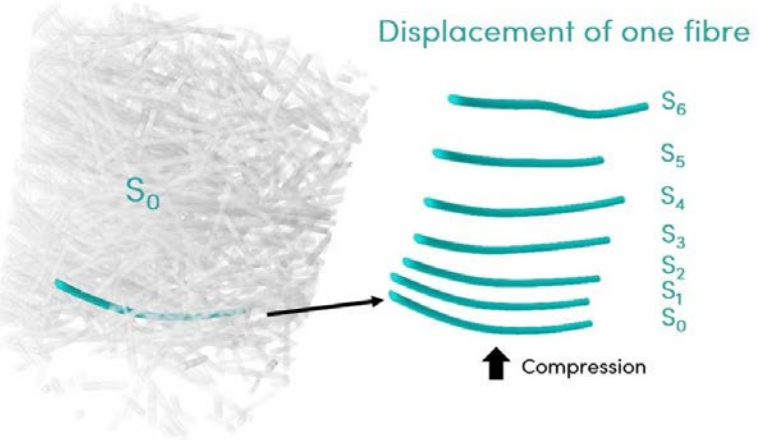

Strength Development. Previously, we reported on the development of a novel automated fibre segmentation algorithm in paper samples. Here we are able to label individual fibres in a sheet, and then quantify them individually. We have built upon this algorithm and have modified the tool to quantify contacts between fibres, leading to an estimate of the relative bonded area in paper. The key scientific challenge is to separate artifacts created from image blur and noise which cause near-contacts to appear as a true contact. We have proposed a novel image analysis methodology to decouple these artifacts and have implemented this in MATLAB. In this reporting period we benchmarked the performance of our code on two simpler data sets, assemblies of spheres and nylon fibres. Critically, our methodology performed well and in the case of spheres, we were able to reproduce theoretical estimates. This increased the confidence in our approach. In the next phase of the work, we benchmarked the performance of the algorithm using nylon fibre networks (as a simpler surrogate to paper samples) during compression.

PROJECT 3.2

A representative image of the motion of an individual fibre in a nylon floc under compression is shown in the previous figure. We successfully resolved and characterized the individual contacts, and, uniquely, confirmed longstanding theoretical work on the number of contacts in random networks.

Chip Impregnation. In the previous reporting period, we impregnated wood chips under conditions typically used in chemimechanical pulping (CMP) and chemithermomechanical pulping (CTMP) and examined the changes in chip morphology. As a reference we also treated chips under hot water hydrolysis (140°C for 60 min). For the CMP type of treatment, aspen chips were impregnated with 1 mol/L sodium sulphite solution at pH of 10 then cooked at 140°C for 60 min. For CTMP type treatment, Aspen chips were impregnated in 0.4 mol/L sodium sulphite at pH of 12 then cooked at 90°C for 30 min. Imaging of these treated chips is currently ongoing. The majority of our effort during this reporting period was spent on developing tools to label the individual lumens and develop a method to measure the wall thickness. Our approach has been successful and the image processing pipeline is shown below. With this code we are able to track individual lumens, and measure local wall thickness and lumen diameter. We find that on average the fibre walls swell, by about 10%, with pulping treatments.

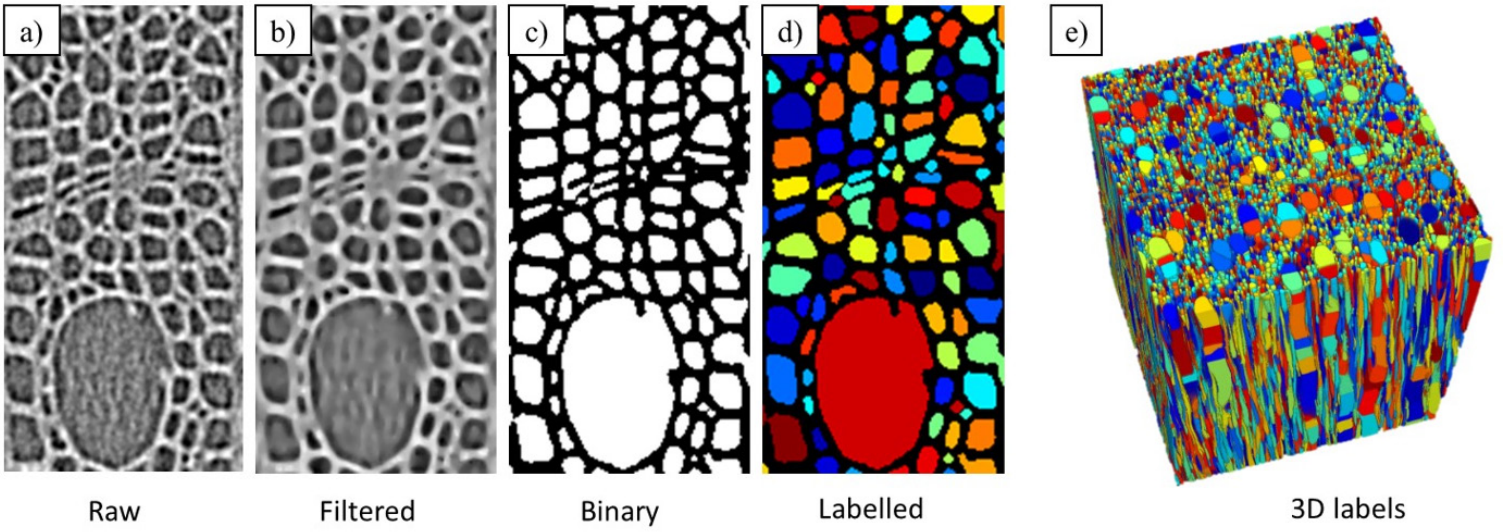

Bulk Preservation. We have recently developed a tool to characterize the "bulk potential" of a papermaking furnish. This tool is based upon profiling the pulping and papermaking process and examining the fraction of fibres which have collapsed. This is highlighted where we compare the wall thickness and diameter of uncollapsed fibres in a paper sample (black dots) to fibre wall thickness and lumen diameter of a wood chip (red dots). Below the green line in this figure, we did not detect any uncollapsed fibres, indicating the minimum wall thickness and diameter of the fibre required to prevent collapse. Seemingly, only fibres with a wall-thickness-to-diameter ratio of greater than about 0.1 remain open during processing. The immediate opportunity with this tool is to profile the mechanical pulping process to determine the loss in bulk.

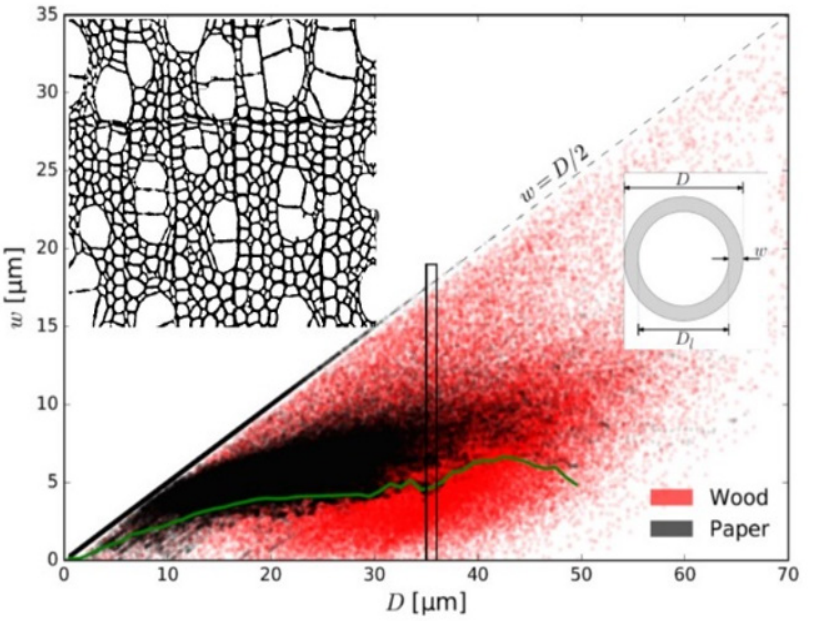

PROJECT 3.2

In this reporting period, we examined this relationship further and visualized fibre collapse during wood chip compression. Here we subjected a hardwood wood chip to uniaxial compression in the x-ray tomograph and measured damage in the fibres as a function of compression. We report that chip compression occurs through a local front region close to the compression platen, inducing fibre buckling which creates local defects in the fibre walls. We speculate that these defects lead to fibre collapse during subsequent processing.

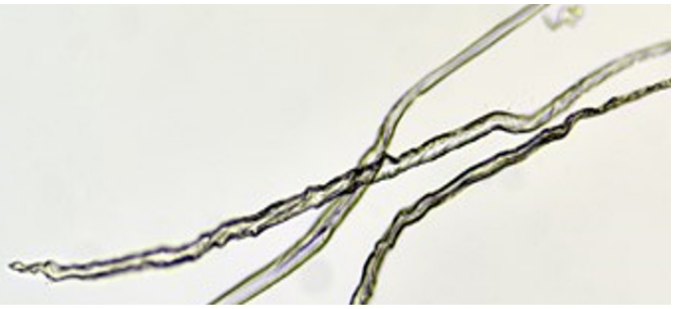

Future Research

In the next phase of the work we will continue image quantification to understand strength development, chip impregnation and bulk preservation.

a. Strength Development: continue benchmarking our algorithm to estimate contacts and relative bonded area. To date, our code works well on idealized structures. We will start to examine performance on more realistic products. We will characterize simpler non-woven products as a first-step to understanding hand sheets.

b. Chip Impregnation: Our algorithm is robust and reliable. We will now use this to understand the rate of impregnation of these chemistries into the chip over the next reporting period.

c. Bulk Potential: We will continue examining defect formation during chip impregnation and compression and relate these to decrease in bulk of the resulting papers.

ERMP PERSONNEL UPDATES

FAREWELLS

Recently the ERMP group has said farewell to postdoctoral fellows Mengqi Fang and Pierre Kasangana. We wish the best to both of them in their new career path, and thank them for all the great contributions in the past year to the ERMP program.

We would like to also highlight Ryan Hlina, undergraduate student, who worked with us during the winter term as a COOP student, supporting our ongoing research and trials at the PPC Pilot plant. We invite you to read about Ryan below.

Ryan Hlina

Ryan grew up on Vancouver Island very involved in outdoor activities such as hiking or community outreach. His time spent in school reflected these interests as he would try and focus on academics that let him spend more time on environmental challenges. Ryan is currently on Co-op, part way through his third year of Chemical and Biological Engineering and has gotten to take part in innovative projects like algae carbon capture in brewing and research into cell grown meats. Ryan assisted Norm with our ongoing research at the papermaking lab, as well as pilot scale trials. We thank Ryan for all his contribution to the program.

NEW ARRIVALS

During the recent months, we have welcomed several new team members, and returning students, at the UBC Pulp and Paper Center. Please read through the brief introductions of our undergraduate COOP students and their backgrounds.

Samuel Brown

Sam returned to the ERMP team, after a succesfull first period last Winter term. He is currently pursuing a BSc in Physics at UBC, and has experience in optics, image processing, and scientific computing. In previous co-op terms, Sam worked as a fuel cell test engineer at Ballard Power Systems and as a biophysics researcher at the Université de Montréal Biophotonics Lab. During the next 4 months, he will continue supporting Project 3.2 with image analysis of wood chip compression effects.

Thomas Clarito

Thomas Clarito is curretly studying engineering at UBC, and has just completed 4th year. Working with ERMP will be his first experience with research. His previous work has been in software development where Thomas learned about cloud computing and data analysis. He is hoping to apply the data analysis skills from his previous experiences here. Thomas enjoyed data analysis and working with cloud computing during his previous coop, and currently enjoys learning about the pulp and paper industry and research.

Stephen Lee

Stephen joined the ERMP team in May 2022. He is currently pursuing a BASc in mechanical engineering at UBC's Okanagan campus, with a minor in computer science. Currently, he is working in the papermaking lab conducting freeness tests, and will eventually be aiding in various facets of material analysis.

PPC UPDATES

Renz Po

Renz is currently pursuing his Bachelor of Science in Microbiology & Immunology at The University of British Columbia. He joined the ERMP program in May 2022 with the aim of supporting the project. A passion for working in the wet lab environment made him find his way into our team (fortunately). Under the supervision of Dr. Rodger Beatson, Dr. Sudipta Kumar Mitra, and Claire Maulit, he hopes to contribute greatly into achieving their research goals.

Priyanshi Shrivastava

Priyanshi is a MITACS globalink intern who joined the ERMP team in May 2022. She is a chemical engineering undergraduate at Birla Institute of Technology, Mesra. Here, she is working under the supervision of Dr. Heather Trajano and PhD student, Mariana. She'll spend the majority of her time at UBC's pulp and paper centre. MFC, the benefits of chemical treatment prior to refining, and the reduction of energy usage in pulping are some of her research interests.

CHBE Research Day at UBC

Research Day is an event for sharing some of the latest scientific and technical contributions in the Chemical and Biological Engineering fields. The CHBE Department at UBC opens its doors to scientists, engineers, and industry partners to take part in the event, which includes posters and oral presentation competitions for graduate students as well as a poster presentation competition for postdoctoral fellows.

We would like to congratulate ERMP PhD student, Mariana Frias de Albuquerque, for winning The Canada Excellence Research Chairs Sponsored Award for **1st Runner Up Poster Presentation.**

Poster Title: Effect of Enzyme Species and Dosage on Production of Microfibrillated Cellulose from Mechanical Pulp Fines.

Congratulations Mariana!

Mariana and Charles Haynes, CHBE department Head

PPC UPDATES

TRIAL UPDATES

Since the last newsletter, we have had multiple pilot plant trials completed at the PPC, led by new Research Technologist Norman Roberts. For the past months, Norm has become familiar with the operation of the refining and fractionation units while training new students and researchers in the correct use of the equipment at the papermaking lab.

Of major note were Matthias' and Samiras' 12 refining trials using two sets of Valmet plates with distinct plate geometries in combination with bar force sensor measurements. To complete this work, 6 remaining trials are planned for the middle of June. Coop students, Thomas Clarito and Stephen Lee, are currently analyzing the fibre qualitative data comprising this large set of trials.

Further trials have been completed with the MR8 Pressure Screens to support our ongoing work involving MFC production and characterization. A large scale fractionation trial using the 0.8 mm screen basket as part of Mariana's work was completed earlier this year, using our source pulp BCTMP (From QRP, West Fraser). Mariana produced enough material for further enzymatic treatments.

Additional refining and fractionation trials are expected during the upcoming months. Feel free to contact Program Manager Daniela Vargas Figueroa if you are interested in accessing our facilities.

Mariana and Norm at the HHL

Samira, Matthias and Norm at the HHL.

PUBLICATIONS

Journal Articles

1. A. Sibellas, J. Drummond, A. Phillion, & D.M. Martinez," Estimating the number of contacts in sedimented fibre assemblies, Progress in Paper Physics, Atlanta (2021)
2. Sibellas, A., Litjens, J., Drummond, J., Phillion, A.B. & Martinez, D.M., "Visualization of monodisperse fibre assemblies during compression" Fundamental Research Society in Pulp and Paper Research, Cambridge (2022)
3. Sibellas, A., Brown, S., Drummond, J., Phillion, A.B. & Martinez, D.M., "Visualization of the Compression of Aspen Wood Chips Using 3D mCT", International Mechanical Pulping Conference, Vancouver (2022)

CONTACTS

You are welcome to contact any of the faculty or staff:

Daniela Vargas Figueroa
Program Manager, UBC
604-827-2390
Daniela.Figueroa@ubc.ca

Mark Martinez
Professor, UBC
604-822-8564
Mark.Martinez@ubc.ca

James Olson
Professor, UBC
604-822-5705
James.Olson@ubc.ca

Rodger Beatson
Professor, BCIT
604-432-8951
Rodger_Beatson@bcit.ca

Laurel Schafer
Professor, UBC
604-822-9264
Schafer@chem.ubc.ca

Peter Wild
Professor, UVic
250-721-8901
PWild@uvic.ca

Bhushan Gopaluni
Professor, UBC
604-827-5668
Bhushan.Gopaluni@ubc.ca

Emily Cranston
Associate Professor, UBC
604-827-0627
Emily.Cranston@ubc.ca

Boris Stoeber
Professor, UBC
604-827-5907
Boris.Stoeber@ubc.ca

Heather Trajano
Associate Professor, UBC
604-827-1823
Heather.Trajano@ubc.ca

Yankai Cao
Assistant Professor, UBC
604-822-2693
Yankai.Cao@ubc.ca

Scott Renneckar
Associate Professor, UBC
604-827-0637
Scott.Renneckar@ubc.ca

André Phillion
Associate Professor, McMaster
905-525-9140 x24046
Philliab@mcmaster.ca

Visit our website www.EnergyReduction.ppc.ubc.ca

PARTNERSHIP IS OUR STRENGTH

The supporting partners of this research program are:

AB Enzymes, Alberta Newsprint Company, BC Hydro, BCIT, Canfor, Catalyst Paper, FPInnovations, Holmen Paper, McMaster University, Meadow Lake Pulp, Millar Western, NSERC, The University of British Columbia Pulp and Paper Centre, The University of Victoria, West Fraser and Valmet.